UNCLASSIFIED

AD NUMBER
AD882075

LIMITATION CHANGES

TO:

Approved for public release; distribution is unlimited.

FROM:

Distribution authorized to U.S. Gov't. agencies only; Test and Evaluation; DEC 1970. Other requests shall be referred to Naval Air Systems Command, Washington, DC 20360.

AUTHORITY

USNSRDC ltr 24 Apr 1974

THIS PAGE IS UNCLASSIFIED

NAVAL SHIP RESEARCH AND DEVELOPMENT CENTER

Washington, D.C. 20034

TWO-DIMENSIONAL TRANSONIC WIND TUNNEL TESTS

OF THREE 15-PERCENT THICK CIRCULATION

CONTROL AIRFOILS

by

Robert J. Englar

AVIATION DEPARTMENT

December 1970

Technical Note AI-182

72

TWO-DIMENSIONAL TRANSONIC WIND TUNNEL TESTS
OF THREE 15-PERCENT THICK CIRCULATION
CONTROL AIRFOILS

by

Robert J. Englar

December 1970   Technical Note AL-182

SUMMARY

Two-dimensional transonic wind tunnel tests were conducted on three
fifteen percent circulation control elliptic airfoils over the range $0.3 \leq M_\infty \leq 0.9$. Model configurations included a pure elliptical shape with both
jet flap and tangential upper surface trailing edge blowing, plus tangen-
tial blowing over an elliptical shape with a rounded trailing edge. Perfor-
mance of the rounded trailing edge configuration was the best of the three
at low speeds, but above $M_\infty = 0.55$, detachment of the Coanda jet caused
rapid performance deterioration. Due to its elongated trailing edge and
associated larger effective radius downstream of the slot, the tangentially
blown pure ellipse was able to extend the jet detachment Mach number to 0.7,
where maximum equivalent lift-to-drag ratios of 22 at C_ℓ of 0.44 were
achieved. The jet flap proved to be inferior to the tangentially blown
configurations in all respects except in its ability as a thrusting, drag-
reducing body.

TABLE OF CONTENTS

LIST OF FIGURES

iii

LIST OF FIGURES (Continued)

LIST OF FIGURES (Concluded)

LIST OF SYMBOLS

A_e slot area, (bh), ft^2

a_j local speed of sound in the jet, ft /sec

A_j nozzle throat area, ft^2

b model span, ft

c model chord, ft

C_d two-dimensional drag coefficient from momentum loss in wake, corrected for additional mass efflux of the jet

$C_{d_{e_1}}$ force-based equivalent drag coefficient, $C_d + C_\mu + C_\mu \dfrac{V_\infty}{V_j}$

$C_{d_{e_2}}$ kinetic-energy-based equivalent drag coefficient, $C_d + \dfrac{C_\mu V_1}{2V_\infty} + C_\mu \dfrac{V_\infty}{V_j}$

C_ℓ two-dimensional lift coefficient

$C_{m_{50}}$ pitching moment coefficient about the half chord

C_p pressure coefficient

C_p^* critical pressure coefficient (corresponding to local M of 1.0)

C_μ momentum coefficient, $\dot{m} V_j/(q_\infty c)$

h slot height at nozzle throat, ft

ℓ/d_{e_1} force-based equivalent lift-to-drag ratio

ℓ/d_{e_2} kinetic-energy based equivalent lift-to-drag ratio

M_{crit} critical Mach number

M_∞ freestream Mach number

M_j jet Mach number

$\dot{m}$ mass efflux, slug/sec

P_∞ free stream static pressure, lb/ft^2

P_{t_∞} free stream total pressure, lb/ft^2

P_{t_d} duct (plenum) pressure, lb/ft^2

q_∞	free stream dynamic pressure, $lb/ft.^2$
r	trailing edge radius, ft
R_e	Reynolds number, based on chord
T_t	total temperature, $^\circ R$
T_j	static temperature in the jet, $^\circ R$
V_∞	free stream velocity, ft /sec
V_j	jet velocity, ft /sec
x/c	dimensionless chordwise station
α	geometric angle of attack, degrees
γ	ratio of specific heats
θ	local angle of jet at exit relative to free stream
δ	chord line camber, ft

INTRODUCTION

Modified elliptic circulation control airfoil sections have been shown subsonically to be very effective generators of high lift coefficients and aerodynamic efficiencies (References 1 and 2). Employing camber and tangential blowing over a rounded trailing edge, these sections have generated lift coefficients greater than 6.0 and efficiencies (equivalent lift-to-drag ratios) above 90 (at $C_\ell \approx 1.0$). These airfoils thus appear quite promising for application to inboard and mid-span blade sections of rotary wing aircraft. However, due to their camber and relatively large thickness-to-chord ratio (20 to 30 percent or greater), their effectiveness at the high speed rotor tip would tend to be reduced.

Examination of the rotor tip flow regime indicates that present high speed helicopter configurations are limited by three main problem areas: compressibility or Mach number effects, retreating blade stall, and blade structural limitations. These criteria lead to the demand for a tip section designed to (1) increase the drag divergent Mach number, (2) maintain good transonic lift coefficient and equivalent lift-to-drag ratio, and (3) control the shock location and closely related boundary layer separation. In addition, the section must still maintain relatively good subsonic characteristics as the retreating blade would be required to operate in the low speed (or even reverse flow) region. It is this requirement to cyclically operate in alternately subsonic and transonic regions which leads to the mechanical and structural complexities of present day rotor systems. It is felt that these problems may be considerably reduced or eliminated by proper design of a circulation control transonic tip section where the necessary cyclic variations are obtained by programmed air ejection over the trailing edge.

The present tests were intended to investigate the transonic properties of a series of relatively thin (15 percent) elliptic sections with several variations in blowing schemes. In particular, it was desired to determine if the impressive subsonic efficiencies of the tangentially blown ellipse could be maintained at high subsonic and transonic speeds, while simultaneously satisfying the requirements mentioned above for a high speed tip section. Previous tests on transonic circulation control airfoils (Reference 3)

with Coanda effect tangential blowing over rounded trailing edges have shown loss of lift augmentation and section efficiency above a Mach number of 0.55 due to detachment of the jet sheet. Therefore, an important aspect of the present tests was to determine if the Mach number for jet detachment could be increased by variation in trailing edge curvature.

MODELS AND TEST APPARATUS

The series of three models used in the two-dimensional transonic test program was constructed in a manner similar to previous subsonic ellipses tested at NSRDC (see References 1 and 2). However, certain additional steps were taken to strengthen the models to withstand the higher transonic loads and to provide a fine surface finish to prevent misrepresentation of boundary layer separation and shock wave formation.

MODELS

The basic configuration for all three models was an uncambered ellipse of 15 percent thickness-to-chord ratio chosen from the critical Mach number (M_{crit}) consideration shown in Figure 1, which is based on a Karmann-Tsien rule extension of potential flow data. It was expected that the required rotor tip lift coefficient would lie in the region $0 \le C_\ell \le 1.0$; thus the best compromise for increased M_{crit} was the 15 percent ellipse. In contrast, the thicker 20 percent ellipse would probably not perform as well in the higher Mach number range where viscous and compressibility effects are strong, while the 10 percent section would fare poorly in the subsonic retreating blade regime.

In addition to the pure 15 percent ellipse, a trailing edge more favorable to subsonic circulation control was chosen, i.e., a circular trailing edge with a radius equal to 4 percent of the chord. As shown in Figure 2, at the higher C_ℓ generated subsonically by this rounded trailing edge, suction peaks (minimum C_p) less than for the pure ellipse were present, while the reverse was true at $C_\ell < 1.0$. These higher peaks at the expected transonic lift coefficients would reduce the critical Mach number of the section. This airfoil was included primarily to investigate the high speed jet detachment phenomenon, and as a representative low speed profile for

2

comparison. A third model employing a jet flap was included for comparison purposes with the tangentially blown configurations.

Figure 3 depicts the geometries of the three two-dimensional models. The pure ellipse and the jet flap were unmodified 15 percent thick ellipse sections sharing a common leading edge with interchangeable trailing edge. Both had an 8 inch chord. The tangentially blown pure 15 percent ellipse (hereafter referred to as the "pure ellipse") had an upper surface tangential slot at 92.4 percent chord from the leading edge, while the jet flap had a lower surface slot aligned 30° to the chord and at the 98.3 percent station. The third trailing edge (to be referred to as the rounded ellipse) had a 0.31 inch radius trailing edge in place of the pure elliptic radius ($r = 0.09$ inch), thus producing a shorter chord of 7.70 inches, an actual thickness of 15.6 percent and a slot location at the 96 percent station. All three models were of 0.25 inch thick fiberglass with a 600 fineness finish. Structural strength as well as trailing edge attachment were provided by a rectangular steel spar, which also served as the forward wall of the blowing plenum chamber in the trailing edge. The slot on the two tangentially blown sections was formed by a steel blade held in place by a series of jack screws which were also used to adjust the slot height. In all three configurations, the plenum exit was carefully designed so that the slot exit was the minimum area throat of a smoothly converging nozzle.

TEST APPARATUS AND TECHNIQUE

The intended two-dimension tests required that a small transonic tunnel be found with air supply for blowing and some means of blockage control for the relatively thick high speed models. A survey of available tunnels (Reference 4) yielded the 12 x 16 inch induction tunnel at the University of Minnesota's Aero Hypersonic Laboratory (previously Rosemount Aeronautical Laboratories). This facility had the advantages of suction on the slotted floor and ceiling to reduce or eliminate blockage, as well as a high pressure air supply (outlet pressures of 1500 psig). In addition, a preceding blown airfoil test conducted in that tunnel by Honeywell Inc., (Reference 3), made available to NSRDC a complete blowing system hookup compatible with the present models, plus a concentric ring

3

strain gage wall balance with minimized effect due to pressure line connections. The tunnel and wall balance are presented in Figures 4 and 5, obtained from Reference 3. This reference also contains very detailed information on the facility, test setup, and a transonic test technique similar to that employed in the present test.

The difficulty in evaluating several tares (wall boundary layer, wall deflection, wall-airfoil interaction and air supply pressure hose influence) for correction of balance data made balance drag data almost meaningless and had a lesser but still noticeable effect on lift. An alternative means was thus used as the primary data source for lift, drag, and moment. All three models were pressure tapped at the center span (as shown in Figure 3) to obtain lift and pitching moment by numerical integration around the airfoil section. Spanwise pressure taps were employed to confirm two-dimensionality of the flow. A total head 54 tube rake was installed approximately 1.5 chord lengths downstream of the model. Drag was calculated by integration of momentum loss in the wake using a Lock-Goldstein compressible technique (References 5 and 6), corrected for the additional mass efflux of the jet as in Reference 2. All pressure data from the model and rake were recorded on a multiple scannivalve readout system with output on tape for computerized data reduction. It should be noted that the integrated drag data already includes the horizontal thrust compenent of the jet as detected by the wake rake. However, integration of the normal force to obtain lift does not include the vertical component C_μ sin θ. This term is difficult to evaluate since θ (the jet angle relative to the freestream direction) is unknown for the curved jet. The largest contribution of this thrust term in percentage of total lift would occur for the case of the jet flap model.

A nominal slot height of 0.010 inch was employed on each of the three trailing edges. The range of duct (plenum) total pressures and associated jet velocities required to produce desired momentum blowing coefficients (C_μ) based on an isentropic expansion to free stream static pressure is depicted in Figures 6 and 7. These related figures are for a 0.01 slot height and 12 inch span (the remainder of the 15 inch model span extending through the balance side plates and attaching to the external air supply lines).

4

Ideal jet velocity (V_j) and mass flow rate ($\dot{m}$) were calculated based on an isentropic expansion from duct total pressure to free stream static pressure (which varied with Mach number since the tunnel stagnation pressure remained constant at atmospheric):

$$V_j = a_j M_j = \sqrt{\gamma R T_j}\ M_j = \left\{ 2RT_t \left(\frac{\gamma}{\gamma-1}\right) \left[1 - \left(\frac{P_\infty}{P_{t_d}}\right)^{\frac{\gamma-1}{\gamma}} \right] \right\}^{\frac{1}{2}}$$

Choked nozzle:
$$\dot{m} = A_j P_{t_d} \sqrt{\frac{\gamma}{RT_t}} \left(\frac{2}{\gamma+1}\right)^{\frac{\gamma+1}{2(\gamma-1)}}$$

Unchoked nozzle:
$$\dot{m} = A_j P_{t_d} \left\{ \frac{2\gamma}{(\gamma-1)RT_t} \left[\left(\frac{P_\infty}{P_{t_d}}\right)^{\frac{2}{\gamma}} - \left(\frac{P_\infty}{P_{t_d}}\right)^{\frac{\gamma+1}{\gamma}} \right] \right\}^{\frac{1}{2}}$$

and
$$C_\mu = \frac{\dot{m} V_j}{q_\infty c}$$

The actual test values varied from the above in that the trailing edge slot deflected under high plenum pressures and nozzle losses existed. To account for this, static tests of the model were conducted and the ratio of measured-to-isentropic mass flow was determined as a function of the pressure ratio P_∞ / P_{t_d}. These ratios were then used to calculate the test values of blowing coefficients.

Plenum air supply was obtained through the high pressure Honeywell lines which were sealed into adaptors on the model endplates by O-rings. These prevented leaks while minimizing any resistance the connections would offer to model pitching moment. Total pressure and temperature in the plenum were measured by internal pressure gage and thermocouple. Tunnel free stream static pressure (P_∞) was measured in the tanks adjacent to the slotted ceiling and floor of the test section, with blockage being reduced or eliminated at higher Mach numbers by proper adjustment of suction out of

these tanks. Test section Mach number and dynamic pressure were determined from the relations

$$M_\infty = \left\{ \frac{2}{\gamma - 1} \left[\left(\frac{P_{t_\infty}}{P_\infty} \right)^{\frac{\gamma-1}{\gamma}} - 1 \right] \right\}^{\frac{1}{2}}$$

$$q_\infty = \tfrac{1}{2} \gamma P_\infty M_\infty^2$$

where free stream total pressure P_{t_∞} was atmospheric.

DESIGN AND TEST CONSIDERATIONS

It was surmised that generation of high equivalent lift-to-drag ratios in the transonic regime could be accomplished if an effective means of drag reduction could be found which did not demand large additional blowing power penalties. The jet flap has been shown (Reference 7) to shift the shock wave location rearward and thus favorably effect shock induced separation and related drag. It also exhibited good thrust recovery. However, the jet angles for desirable drag characteristics were frequently different from those for good lift augmentation. On the other hand, tangential blowing over a rounded trailing edge was superior subsonically to the jet flap in lift augmentation and equivalent lift-to-drag ratio, but began to lose this superiority transonically due to jet detachment. A compromise between these two configurations was needed and the design criteria became one for favorable transonic lift augmentation and drag reduction (including thrust augmentation). It was felt that this could be accomplished with an elongated trailing edge, i.e., a larger radius after the slot but preceding a relatively small trailing edge radius. The pure 15 percent ellipse with slot at 92.4 percent chord met this criteria, even though its shape was probably not the optimum.

Size of the model was chosen from consideration of Reynolds number effect on scaling. Reference 8 indicates that $(1.5 \text{ to } 2) \times 10^6$ was the

6

minimum Reynolds number to represent transition and shock-boundary layer interaction phenomenon characteristic of full scale. An 8 inch chord provided Reynolds numbers above this limit throughout the Mach number range above 0.35 (see Figure 8). Natural (free) boundary layer transition was allowed since full scale Reynolds number was expected to be of the same order of magnitude as the model values. The range of momentum coefficients used ($0 \le C_\mu \le 0.08$) was based on an upper limit of 45 psig plenum pressure, above which pressure seals in the model and supply connection had leaked. The range of indicated geometric angle of attack was small, $0^o \le \alpha \le 2^o$ (which was found to be in actuality $-1.2^o \le \alpha \le 0.8^o$) with practically all of the runs being made at $\alpha = -1.2^o$ (actual). The discrepancy is indicated and actual geometric α was due to misalignment of the model relative to the angle of attack setting reference.

DISCUSSION

ROUNDED TRAILING EDGE ELLIPSE

Test were conducted on the 15.6 percent thick rounded trailing edge ($r/c = 0.04$) configuration at $\alpha = -1.2^o$. Lift, drag and moment data are presented in Figures 9 through 20. At Mach numbers of 0.5 and lower, lift variation with blowing showed the characteristic subsonic trend, i.e., continual increase with no apparent drop off at higher values of C_μ (Figures 9 and 10). At higher Mach numbers, ($M_\infty \ge 0.6$) maximum lift coefficient was reached and soon followed by a decrease in C_ℓ with added blowing. The critical Mach number at which this "C_μ stall" began was approximately 0.55, very close to the same phenomenon found in Reference 3. That related study attributes the lift loss to detachment of the Coanda jet from the rounded trailing edge and immediate decrease in circulation.

Figure 11 and 12 depict the variation of lift coefficient and lift augmentation ($\Delta C_\ell / \Delta C_\mu$) with jet velocity ratio (V_j/V_∞) and the associated effect of nozzle choking. Although the lift coefficient continued to increase beyond the choken ($M_j = 1.0$ in the nozzle throat) value of V_j/V_∞, the lift augmentation began to drop off rapidly.

7

Drag showed an even more pronounced variation than lift with increase
in blowing and Mach number (Figures 13 and 14). For $M_\infty \geq 0.4$, an intial
decrease in C_d with increased blowing was followed by a rapid rise in drag.
Analysis of the associated pressure distributions showed reductions in the
trailing edge suction peaks with increase in Mach number in the regime where
this drag rise occurred, thus again indicating jet detachment as the cause
of deterioration of model performance. At $M_\infty \doteq 0.9$, appearance of upper and
lower surface shocks produced a large wave drag contribution to C_d. Associated
with the jet detachment phenomenon was the progressive loss of drag reduction
with increased Mach number. Figure 15 depicts this trend, where the drag
reduction factor is indicative of an increase (positive $\triangle C_d / \triangle C_\mu$) or
decrease in drag coefficient relative to the unblown value. In addition,
increased blowing above the critical Mach number showed little or no effect
on the shock location (Figure 16). Associated lift and drag data are pre-
sented in the drag polar (Figure 17), while the effect of trailing edge
suction peaks due to higher C_μ on pitching moment at the half chord is shown
in Figure 18.

Model performance was best indicated by an equivalent lift-to-drag
ratio which included in the drag term a penalty for blowing. This enabled
the blown airfoil to be compared in efficiency to an unblown configuration.
A simplified equivalent drag coefficient (essentially a force-based coeffi-
cient) could be defined as

$$C_{d_{e_1}} = C_d + C_\mu + \frac{\dot{m}V_\infty}{q_\infty c} = C_d + C_\mu + C_\mu \frac{V_\infty}{V_j}$$

where the third term on the right is an intake penalty described in more
detail in Reference 2. Using this parameter the rounded trailing edge
yielded a maximum ℓ/d_{e_1} of 30 at $M_\infty = 0.4$ and $C_\ell = 0.96$ (Figure 19). A more
appropriate equivalent C_d was derived for kinetic energy and power required
to produce the necessary blowing:

$$K.E. = \tfrac{1}{2}mV_j^2$$

$$P = \frac{\triangle K.E.}{\triangle t} = \frac{\tfrac{1}{2}\triangle mV_j^2}{\triangle t} = \tfrac{1}{2}\dot{m}V_j^2$$

8

Then the total equivalent drag was

$$d_{e_2} = d + \frac{\frac{1}{2}\dot{m}V_j^2}{V_\infty} + \dot{m}V_\infty$$

or in coefficient form

$$C_{d_{e_2}} = C_d + \frac{\frac{1}{2}\dot{m}V_j^2}{V_\infty\, q_\infty\, c} + \frac{\dot{m}V_\infty}{q_\infty c} = C_d + C_\mu \frac{V_j}{2V_\infty} + C_\mu \frac{V_\infty}{V_j}$$

where C_d was the momentum drag coefficient as measured by the wake rake.

The latter parameter (ℓ/d_{e_2}) is preferred for comparison to other airfoils, but requires that the jet velocity be known. This parameter reduced the maximum ℓ/d_{e_2} to 25.9 at $M_\infty = 0.4$, with efficiencies of 15 or less in the Mach number range $M_\infty \geq 0.55$ (Figure 20).

PURE ELLIPTICAL TRAILING EDGE.

The 15 percent thick pure elliptic section with tangential blowing was tested primarily at $\alpha = -1.2°$ (for comparison to the preceding model) with several additional runs at $\alpha = 0.8°$. At low Mach number, the Coanda jet was not as effective over this smaller trailing edge radius $(r/c = 0.01125)$, yielding maximum lift coefficients of 0.91 at $\alpha = -1.2°$ (Figure 21), about half that of the rounded ellipse (Figure 9). However, at $M_\infty \geq 0.7$, C_ℓ was twice that obtained by the rounded trailing edge. In addition, the maximum lift peaks occurred at progressively greater Mach number with decrease in C_μ (Figure 22); whereas for the rounded ellipse, maximum C_ℓ always occurred at $M_\infty = 0.3$ (Figure 10). The limited amount of data at $\alpha = 0.8°$ showed a C_ℓ increase at $M_\infty = 0.7$ of as much as 36 percent with the 2° angle of attack change. The effects of slot choking on lift and lift augmentation were not as noticeable as for the rounded ellipse. Figures 23 and 24 indicate that both C_ℓ and $\Delta C_\ell / \Delta C_\mu$ continued to rise beyond the choking value of V_j/V_∞. A maximum lift augmentation of 43 was realized at $M_\infty = 0.7$ for the pure ellipse, comparable to a similar maximum for the rounded model which was

9

reached at $M_\infty = 0.3$. The pure ellipse's lifting characteristics at higher M_∞ thus appeared superior, a. further emphasized by the comparisons of Figure 25.

Drag characteristics also showed an improvement with the elongated trailing edge. At Mach numbers less than 0.9, an increase in blowing was accompanied by a drag reduction (Figures 26, 27) very similar to trends characteristically exhibited by a jet flap. The drag rise with increased C_μ experienced by the rounded ellipse was eliminated except at $M_\infty = 0.9$, where, before the rise occurred, C_d was favorably reduced with blowing. This latter observation was due to the rearward movement of the upper surface shock with an increase in blowing (Figure 28). A rearward shock movement of 20 percent of the chord was possible with a C_μ increase of 0.0069; additional blowing above that did not relocate the shock. Drag reduction was considerably improved over the rounded ellipse. Figure 29 indicates reduction with increased C_μ at all Mach numbers, although at 0.9 an initial large reduction at very low C_μ was rapidly followed by a reversed trend which pointed towards a net drag increase for C_μ above 0.02. Correlated drag and lift data are presented in the drag polar of Figure 30 while Figure 31 presents variation in half chord moment coefficient with C_μ.

Section performance was again indicated by the two equivalent lift-to-drag ratios (Figures 32, 33). Considering the efficiency based on kinetic energy, the pure ellipse yielded a maximum (ℓ/d_{e_a}) of 22.6 at $M_\infty = 0.7$, almost 3.3 times greater than the rounded ellipse at the same speed, and only slightly less than the rounded edge's maximum at $M_\infty = 0.4$. The higher speed superiority of the pure ellipse over the rounded version in lift, drag, and efficiency was thus well demonstrated.

JET FLAP

The 30° deflection jet flap on the 15 percent thick elliptic section was tested at $\alpha = -1.2^\circ$. Generated lift coefficients (Figures 34 and 35) were considerably smaller than either of the tangentially blown models; maximum C_ℓ was roughly half that of the pure ellipse and 30 percent of the rounded ellipse maximums. However, the jet flap did not experience the "C_μ stall" phenomenon of the tangential models, probably because the jet was not detachable from the trailing edge. The jet also fixed the rear

10

stagnation point, and thus reduced the supercirculation capability of the airfoil. It was effectively a thrust producer, and its effect on drag reduction is shown in Figures 36 through 38, where the trends are similar to the pure ellipse for $M_\infty \leq 0.8$ and $C_\mu < 0.025$. At $M_\infty = 0.9$, drag continued to be reduced by additional blowing, a trend not present for the tangential models. Pressure distributions at this Mach number (Figure 39) indicated that there was some movement (about 5 percent chord) of the upper surface shock with C_μ variation and the lower surface shock moved rearward approximately 5 percent of the chord also. The lack of high trailing edge suction peaks led to a large reduction in the negative pitching moment typically generated by tangential blowing (Figure 40). Figure 41 depicts the jet-flap lift-drag relationship.

In spite of the large drag reduction from the unblown case, the overall efficiencies of the jet flap were low due to the lack of lift augmentation (Figures 42, 43). A maximum l/d_{e_2} of about 8 was generated at $M_\infty = 0.4$ (and $C_l = 0.26$), with lesser values at high Mach numbers, all of which were considerably smaller than for the preceding models.

COMPARISON

Characteristics of the blown sections can best be summarized by direct comparison of the three models. Maximum lift generated for $C_\mu \leq 0.08$ (due to model limitations) is shown in Figure 44, where the subsonic lifting capability of the rounded ellipse yielded to the better transonic properties of the pure ellipse above $M_\infty = 0.55$. The jet flap configuration tested was not competitive in either speed regime. Combining Figure 44 with the drag characteristics, Figure 45 presents the efficiency factor l/d_{e_1}, where again the rounded trailing edge was superior at $M_\infty \leq 0.5$ and the elongated trailing edge was preferred above $M_\infty = 0.5$. The data for the jet flap indicated a weakness of the force-based l/d_{e_1} parameter. The unexpected high efficiency at $M_\infty = 0.3$ was due to the large negative drag produced by a momentum coefficient of similar magnitude (but positive), the sum of the two approaching zero and inflating the parameter. The more meaningful parameter (l/d_{e_2}) avoided this difficulty due to the V_j/V_∞ term in the denominator, and thus the curves of Figure 46 were more indicative of the trend in efficiency. Again the pure ellipse was the most efficient above $M_\infty = 0.55$ (with its

11

maximum at $M_\infty = 0.7$). Lift coefficients associated with these maximum efficiencies (Figure 47) remained almost constant for the pure ellipse up to $M_\infty = 0.7$, while the rounded configuration reached its maximum at $M_\infty = 0.4$ and dropped off rapidly. Associated blowing coefficients (Figure 48) were on the order of $C_\mu \leq 0.02$ for the pure ellipse above $M_\infty = 0.5$ and $C_\mu \leq 0.03$ for the rounded trailing edge below $M_\infty = 0.5$, indicating a relatively low maximum blowing requirement of $C_\mu \leq 0.03$ throughout the entire Mach number range.

CONCLUSIONS

Transonic tests conducted over the range $0.3 \leq M_\infty \leq 0.9$ on a series of three circulation control ellipse airfoils indicated that high speed performance was heavily dependent on maintaining supercirculation primarily by keeping the trailing edge Coanda jet attached. Comparison of experimental results also gave the following conclusions:

- Below $M_\infty = 0.55$, the rounded ellipse configuration was the most favorable of the three, developing the highest lift coefficient, lift augmentation, and aerodynamic efficiency. At higher Mach numbers a rapid drag increase with blowing, apparently resulting from Coanda jet detachment and loss of circulation, caused considerable deterioration in overall section performance of this model.

- The pure 15 percent ellipse with tangential blowing displayed superior high speed characteristics in the range $0.55 \leq M_\infty \leq 0.9$. Due to the elongated trailing edge, the model was relatively free of jet detachment effects up to $M_\infty = 0.7$ and generated greater lift and aerodynamic efficiency, plus reduced drag. The rearward movement of the upper surface shock was beneficial in the latter respect.

- The 30° jet flap configuration was the least effective section of the three, showing promise only in drag reduction (due to its thrusting ability) and lack of lift drop off with increased blowing (although net lift augmentation was small).

12

- For the entire Mach number range, maximum aerodynamic efficiency was obtained at $C_\mu \leq 0.03$; this was reduced to $C_\mu \leq 0.02$ by the pure ellipse at $M_\infty > 0.55$.

The results indicate that the elongated trailing edge was an effective high speed circulation control trailing edge, but that future work should be done to optimize the tangentially blown configuration and extend its range of maximum effectiveness beyond $M_\infty = 0.7$. Of primary importance is a need to understand the phenomenon of high speed Coanda jet detachment and effects upon it of upper surface boundary-layer shock interaction and supersonic expanded flow downstream of the choked nozzle.

Aviation Department
Naval Ship Research and Development Center
Washington, D.C. 20034
October 1970

13

ACKNOWLEDGEMENT

REFERENCES

1. Williams, R.M. Some Research on Rotor Circulation Control. IN CAL/AVLABS Symposium: Aerodynamics of Rotary Wing and V/STOL Aircraft. 3rd, Buffalo, N.Y., Jun 1969. Proceedings, Vol. 2.

2. Williams, Robert M. and Harvey J. Howe. Two Dimensional Subsonic Wind Tunnel Tests on a 20 Percent Thick, 5 Percent Cambered Circulation Control Airfoil. Wash., Aug 1979. 22 l. incl. illus. (Naval Ship Research and Development Center. Tech Note AL-176)

3. Kizilos, A.P. and R. E. Rose Experimental Investigations of Flight Control Surfaces Using Modified Air Jets. St. Pual, Minn., Nov 1969. 154 p. incl. illus. (Honeywell, Inc. Document 12055-FR1. Contract N00019-67-C-0260) (DDC AD 864-2716)

4. Congressional House Committee on Appropriations. National Wind-Tunnel Summary (U). Wash., 1967. [132] p. (DDC AD-390318)   CONFIDENTIAL

5. Hilton, William F. High-Speed Aerodynamics. N.Y., Longmans, Green, 1951. 598 p.

6. Lock, C.N.H., William F. Hilton and Sidney Goldstein. Determination of Profile Drag at High Speeds by a Pitot Traverse Method. London H.M.S.O., n.d. 39 p. incl. illus. (Great Brit. Aeronautical Research Council. R & M 1971. 4709, Sep 1940)

7. Grahame, W.E. and J.W. Headley. Jet Flap Investigation at Transonic Speeds. W-PAFB, Feb 1970. 76 p. incl. illus. (Flight Dynamics Lab. Tech. Rpt. 69-117) (Northrop Corp. Contract F33615-69-C-1429)

8. Pearcey, Herbert H., C.S. Sinnott and J. Osborne. Some Effects of Wind Tunnel Interference Observed in Tests on Two-Dimensional Aerofoils at High Subsonic and Transonic Speeds. Paris, 1959. 61 p. incl. illus. (Advisory Group for Aerospace Research and Development. Rpt. 296).
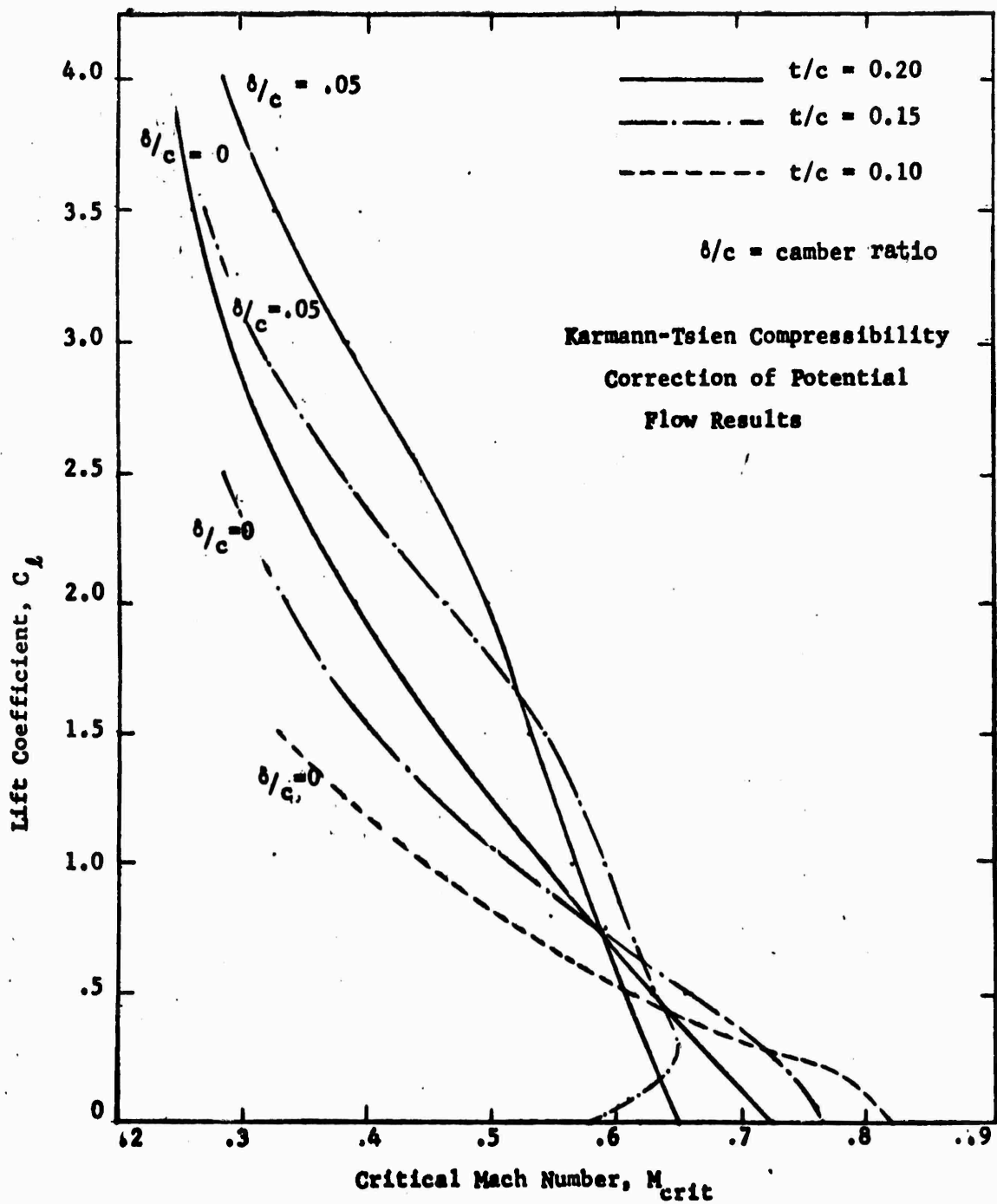
Figure 1 - Critical Mach Number of Ellipses at $\alpha = 0^\circ$

Legend:
- $t/c = 0.20$
- $t/c = 0.15$
- $t/c = 0.10$

δ/c = camber ratio

Karmann-Tsien Compressibility
Correction of Potential
Flow Results

Axis labels: Lift Coefficient, C_ℓ (vertical); Critical Mach Number, M_{crit} (horizontal)

Curve labels: $\delta/c = .05$, $\delta/c = 0$

16
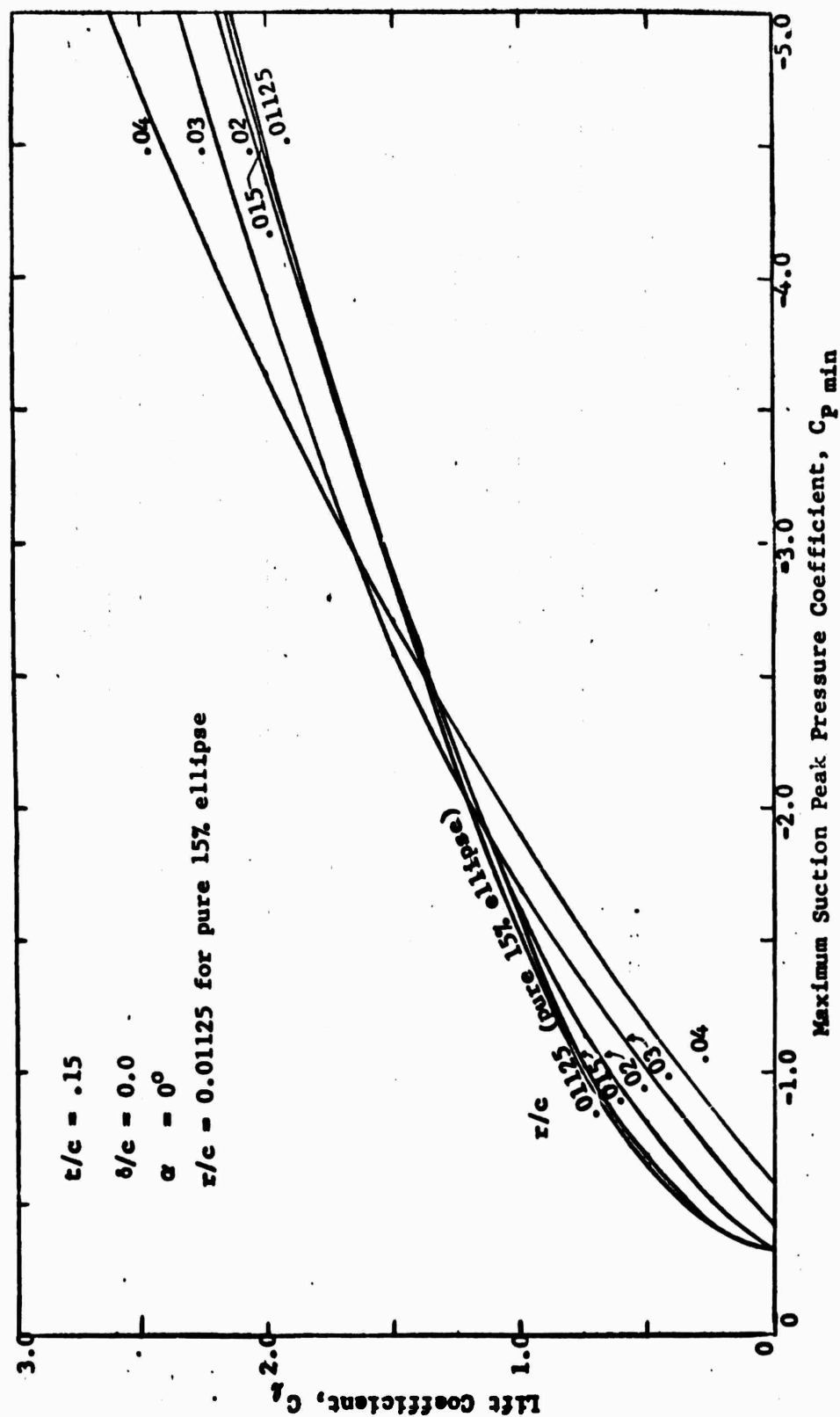
Figure 2 - Effect of Rounded Trailing Edge Variation on Maximum Suction Peaks (Incompressible)

17

dimensions in inches

8.00

7.86
7.70

7.39

4.75

4.00

0.00

0.25" Fiberglass with epoxy resin surface coat

Jet Flap Trailing Edge

Steel Blade

Plenum

Spar

slot adjustment screws

Pressure Taps

Interchangeable Leading Edge

Rounded Ellipse Trailing Edge

Pure Ellipse Trailing Edge

8.00

7.39
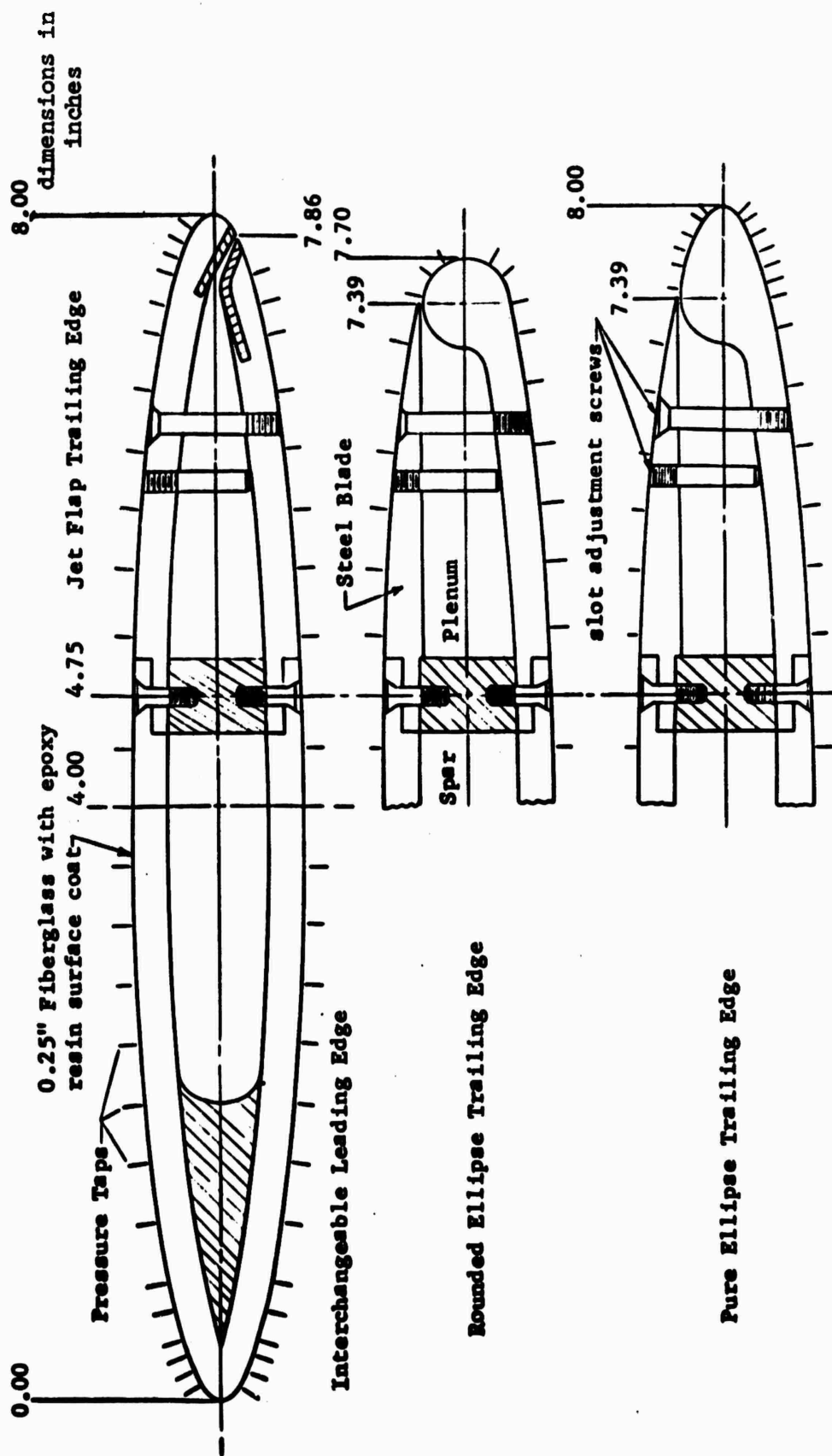
Figure 3 - Transonic Model Geometries
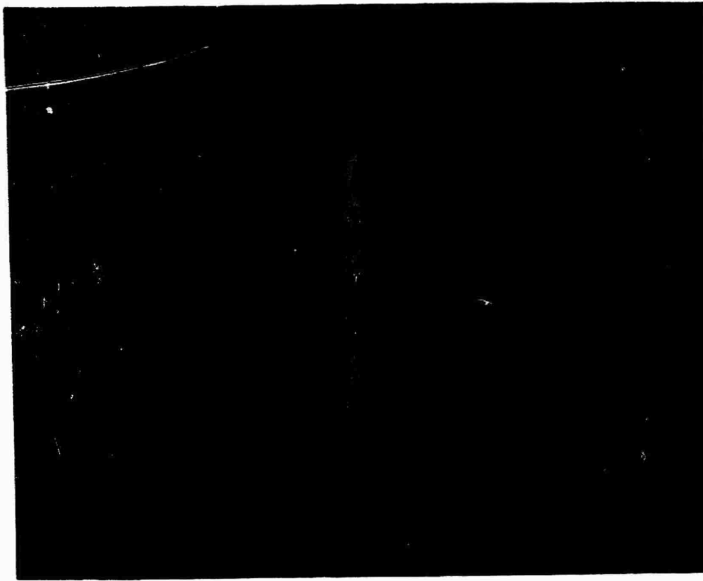
(a) Internal view showing model, balance system disc, and slotted floor & ceiling

(b) External View, looking upstream

Figure 4 - Transonic Wind Tunnel and Associated Test Equipment
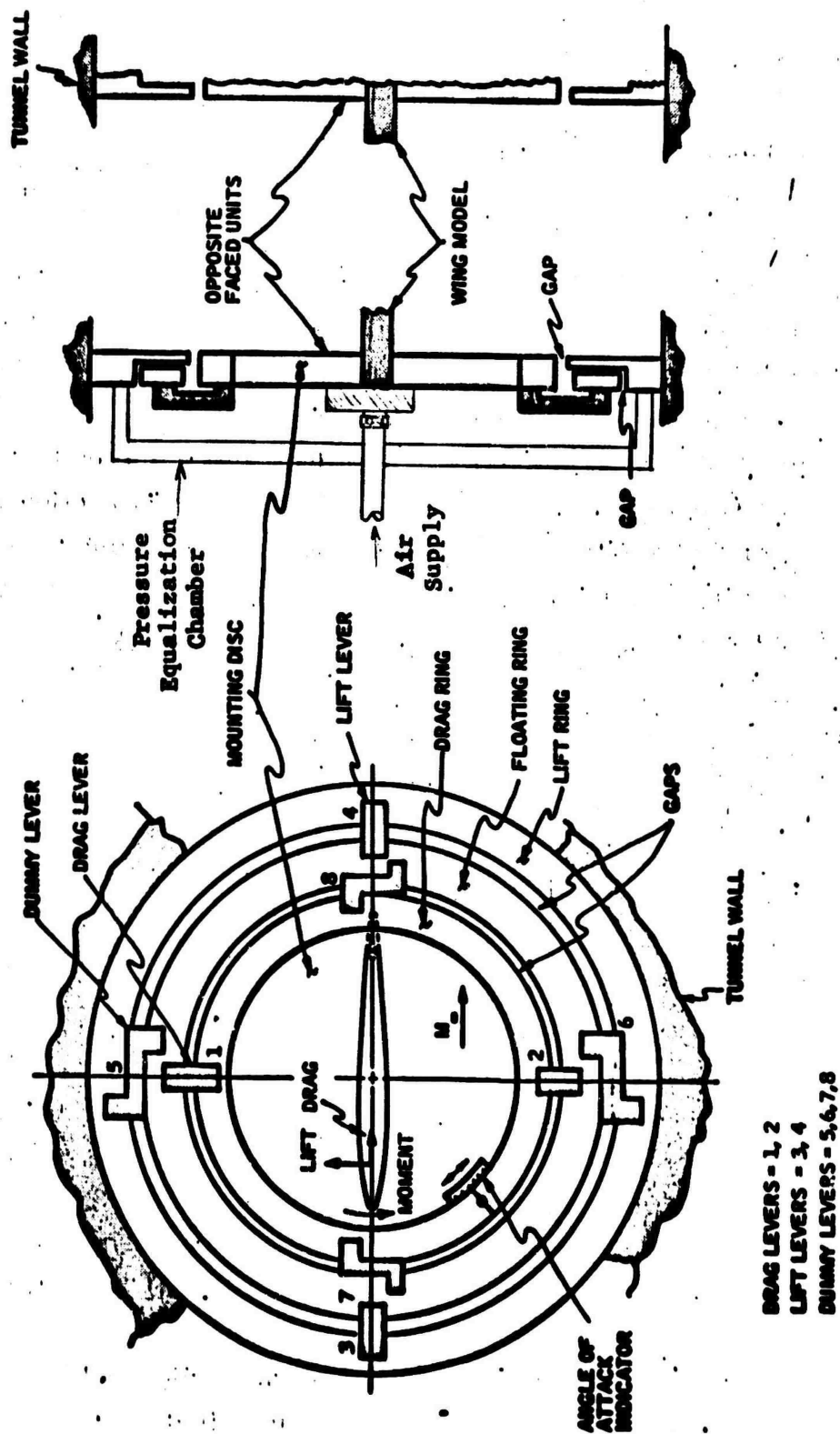
Figure 5 - Concentric Ring Force Balance Schematic
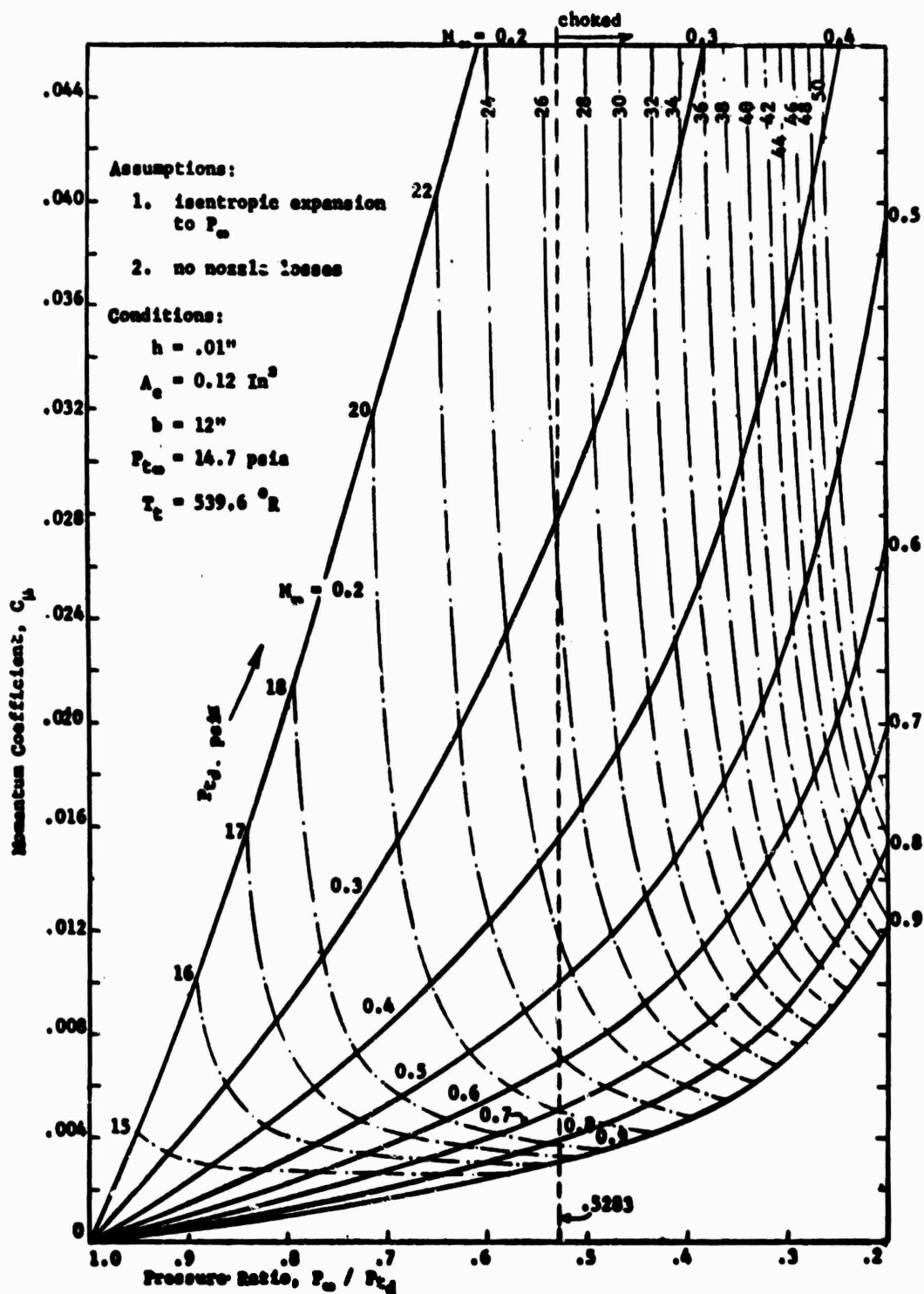
Figure 6 - Pressure Ratio Requirement for 0.01 Inch Slot Height
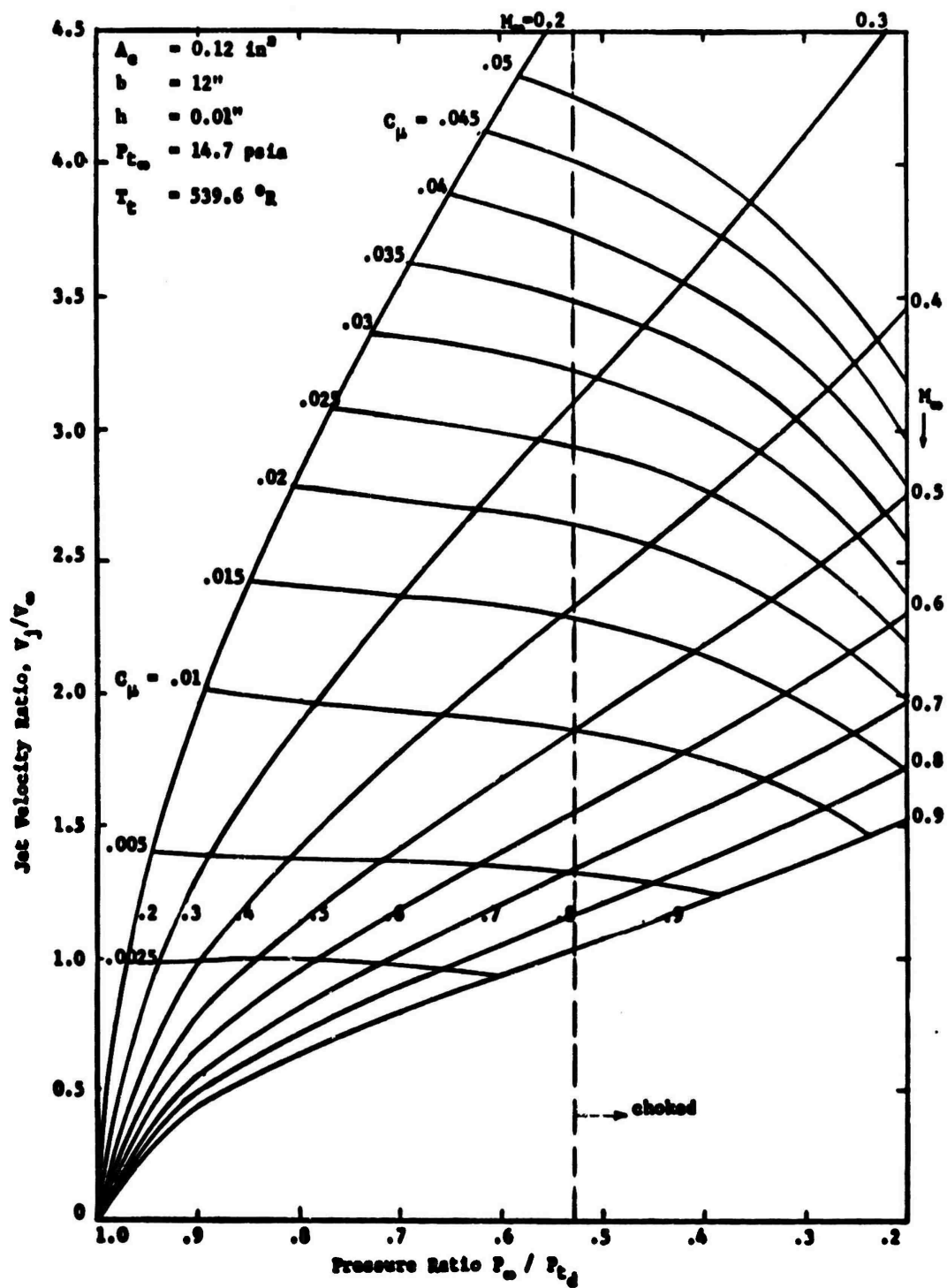
Figure 7 - Jet Velocity Ratio Resulting From 0.01" Slot Height and Variation in Pressure Ratio
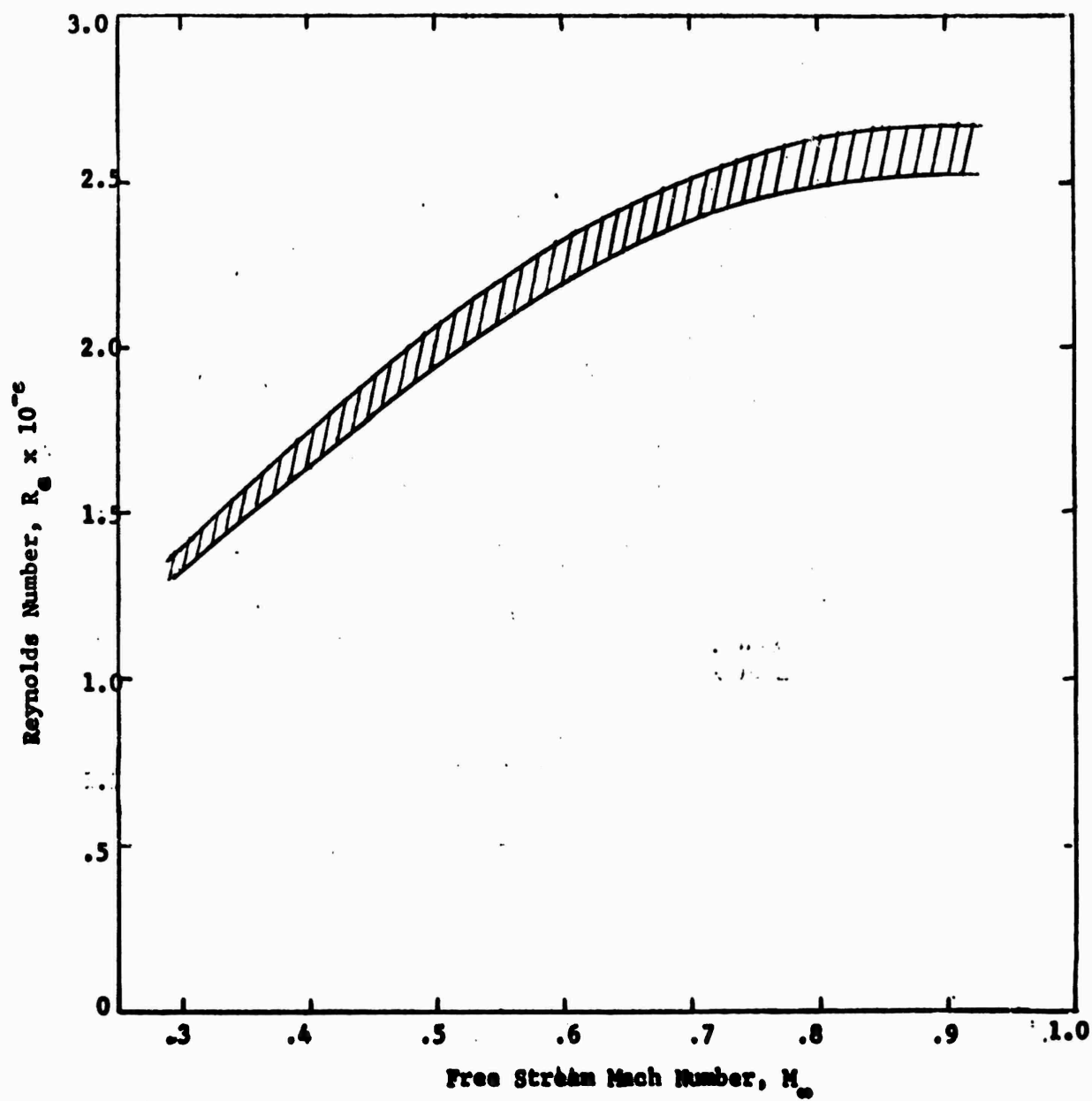
Figure 8 - Test Reynolds Number Range Based on Model Chord
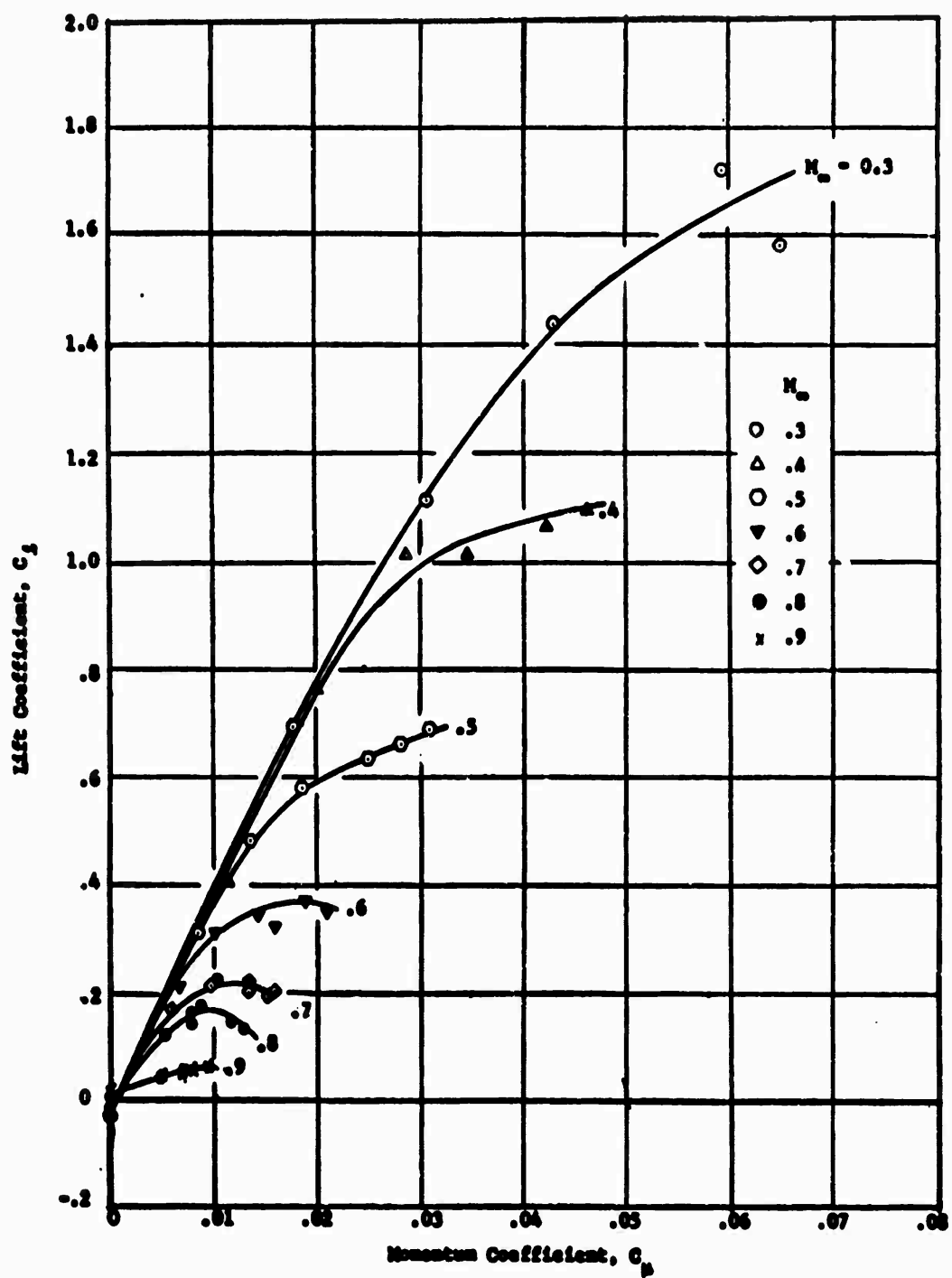
Figure 9 - Lift Variation with Momentum Coefficient
For Rounded Ellipse
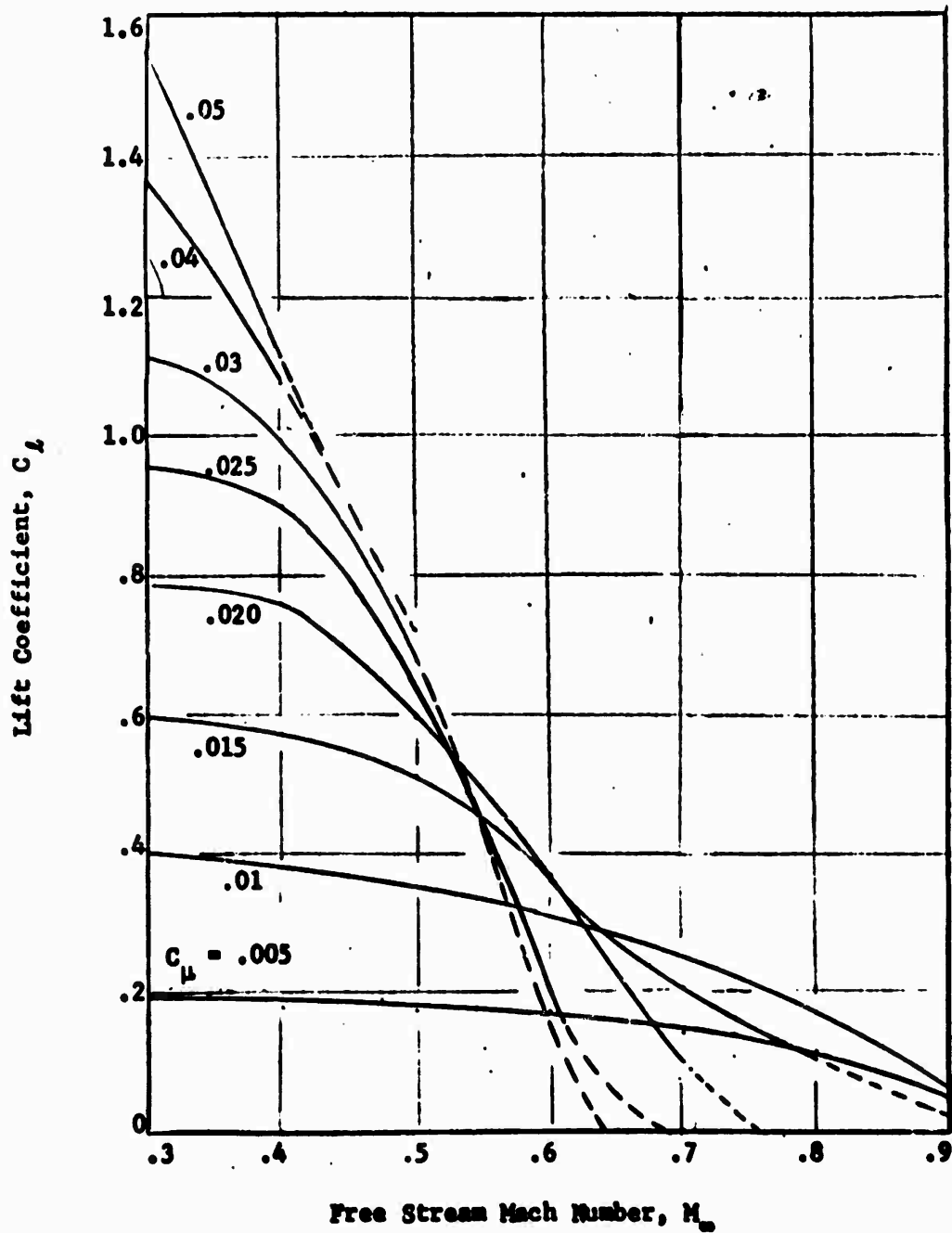
Figure 10 - Lift Variation with Mach Number
for Rounded Ellipse
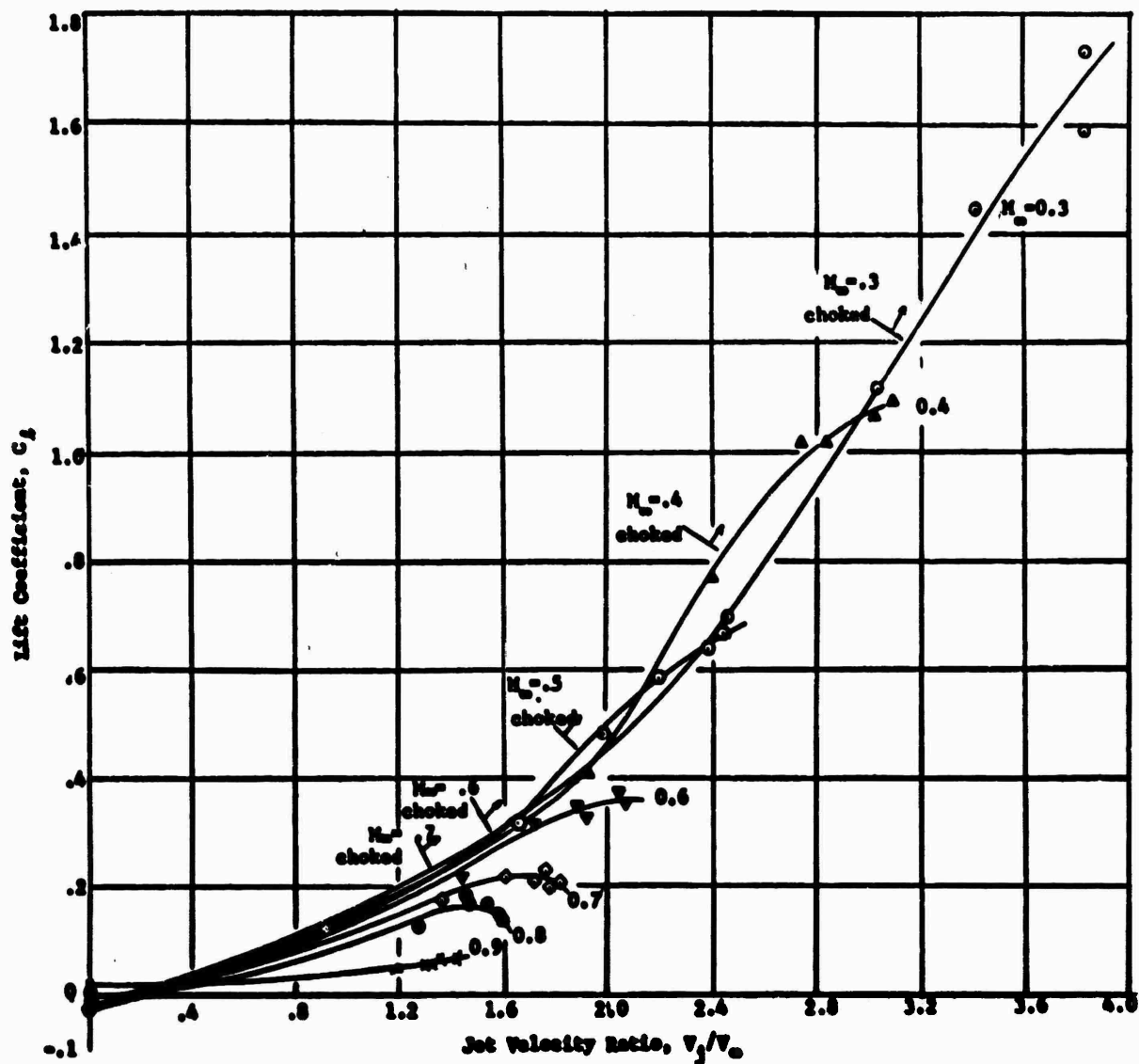
Figure 11 - Lift Variation with Jet Velocity for Rounded Ellipse

26
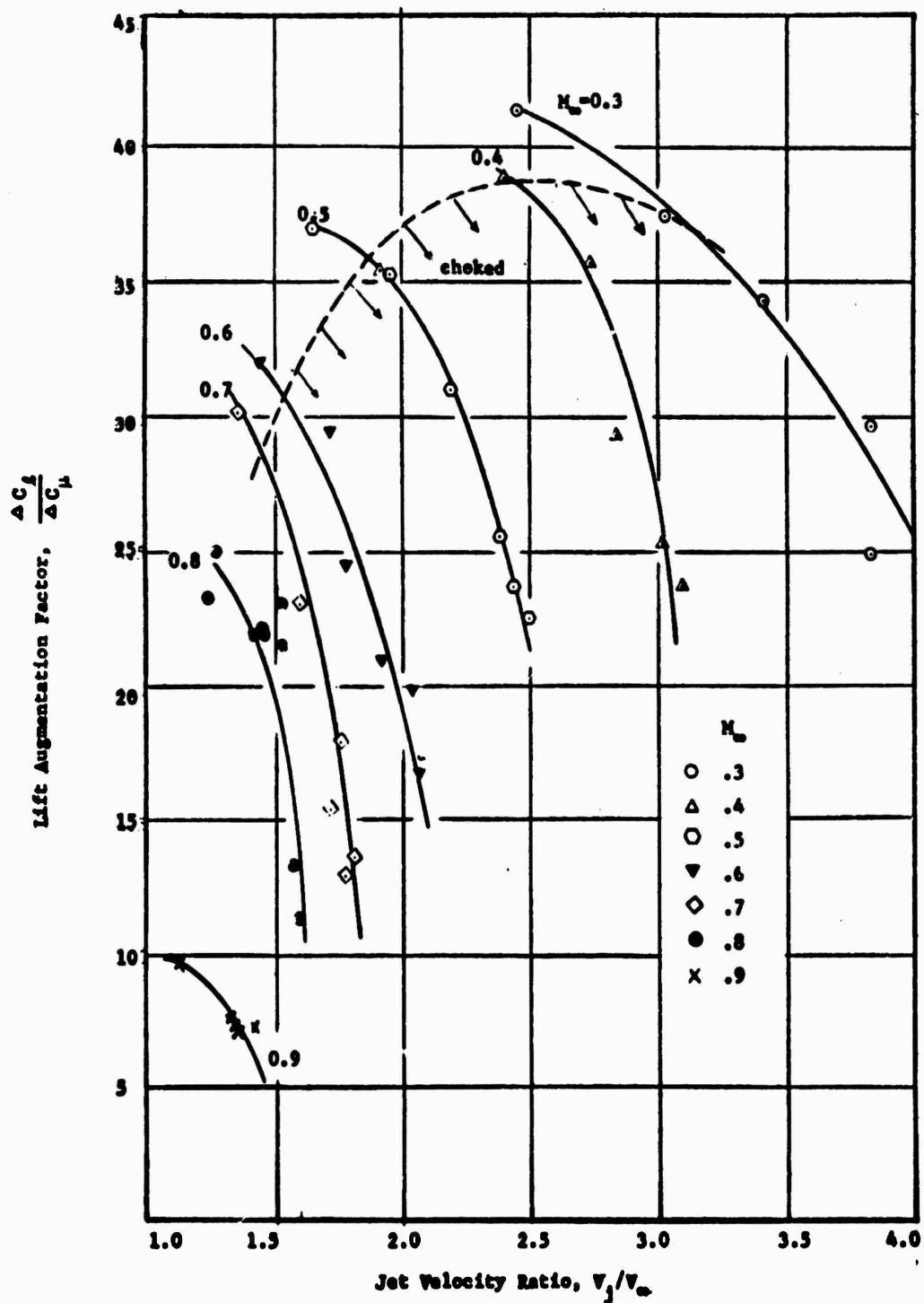
Figure 12 - Variation in Lift Augmentation with Jet Velocity
For Rounded Ellipse

.08

.06

.04

.02

0

-.02

-.04

Drag Coefficient, C_d

M_∞

O .3
△ .4
O .5
▼ .6
◇ .7
● .8
× .9

.9

.8

.7

.6

.5

.4

$M_\infty = .3$

0   .02   .04   .06   .08

Momentum Coefficient, C_μ
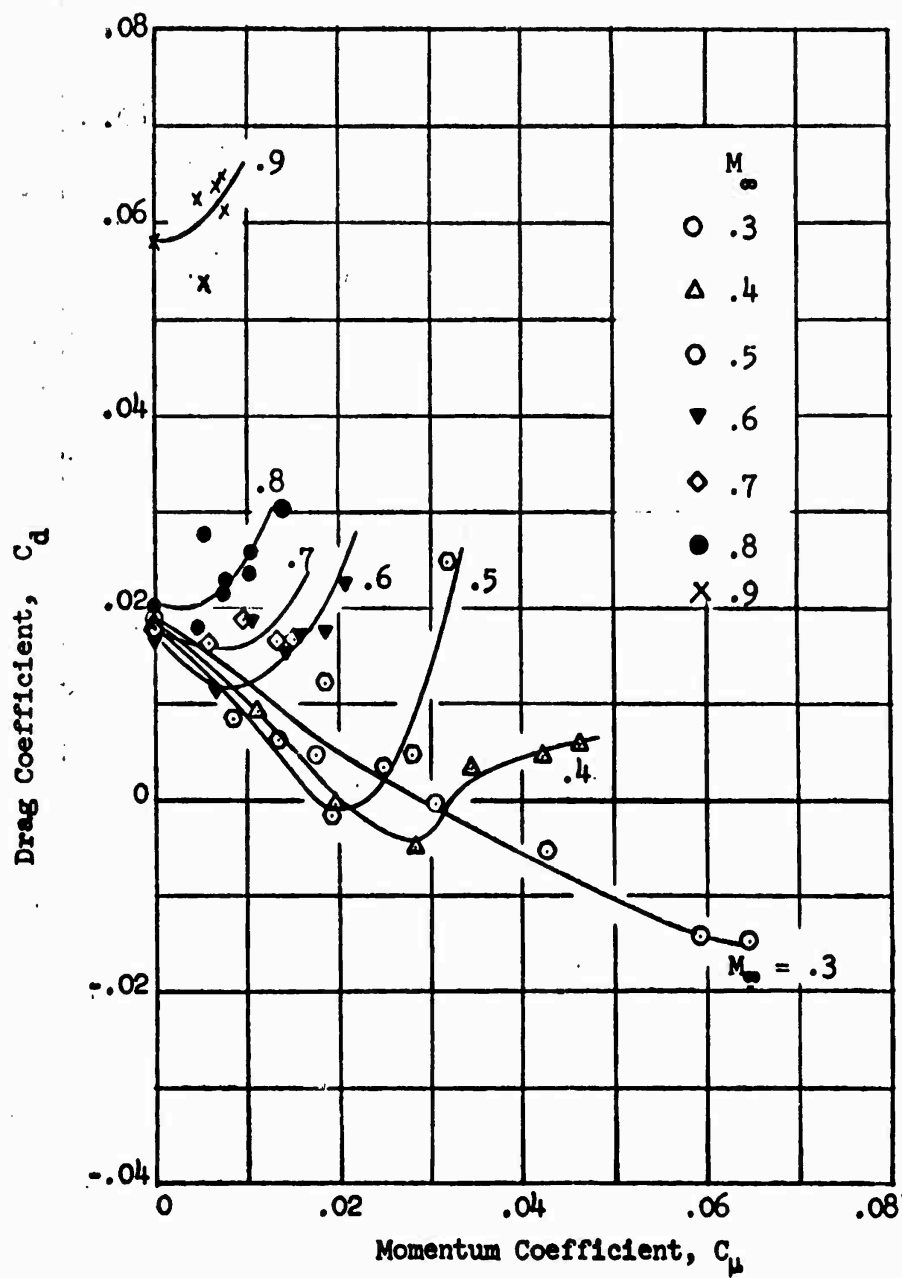
Figure 13 - Drag Variation With Momentum Coefficient For
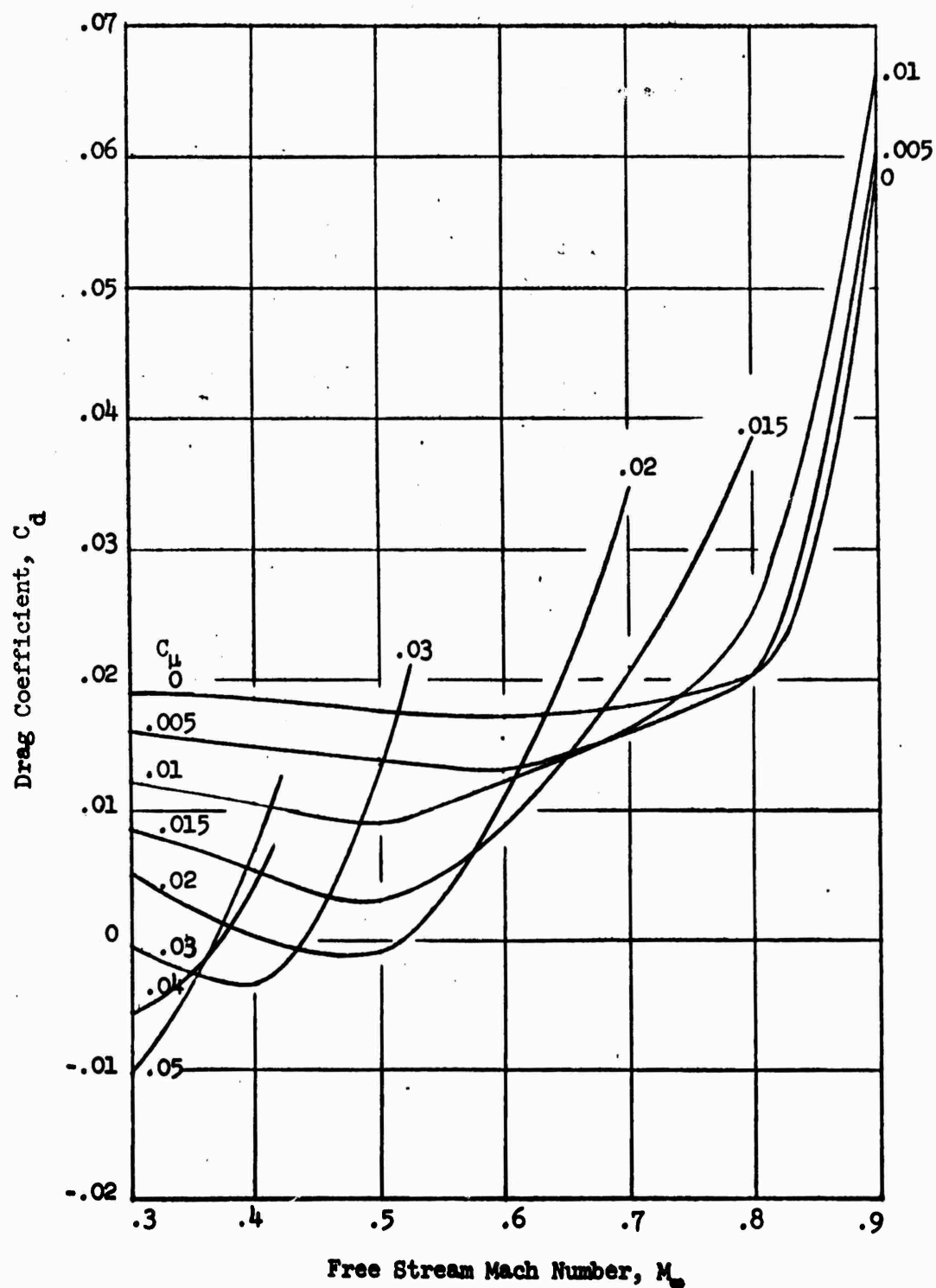
Rounded Ellipse

Figure 14 - Drag Variation with Mach Number for Rounded Ellipse
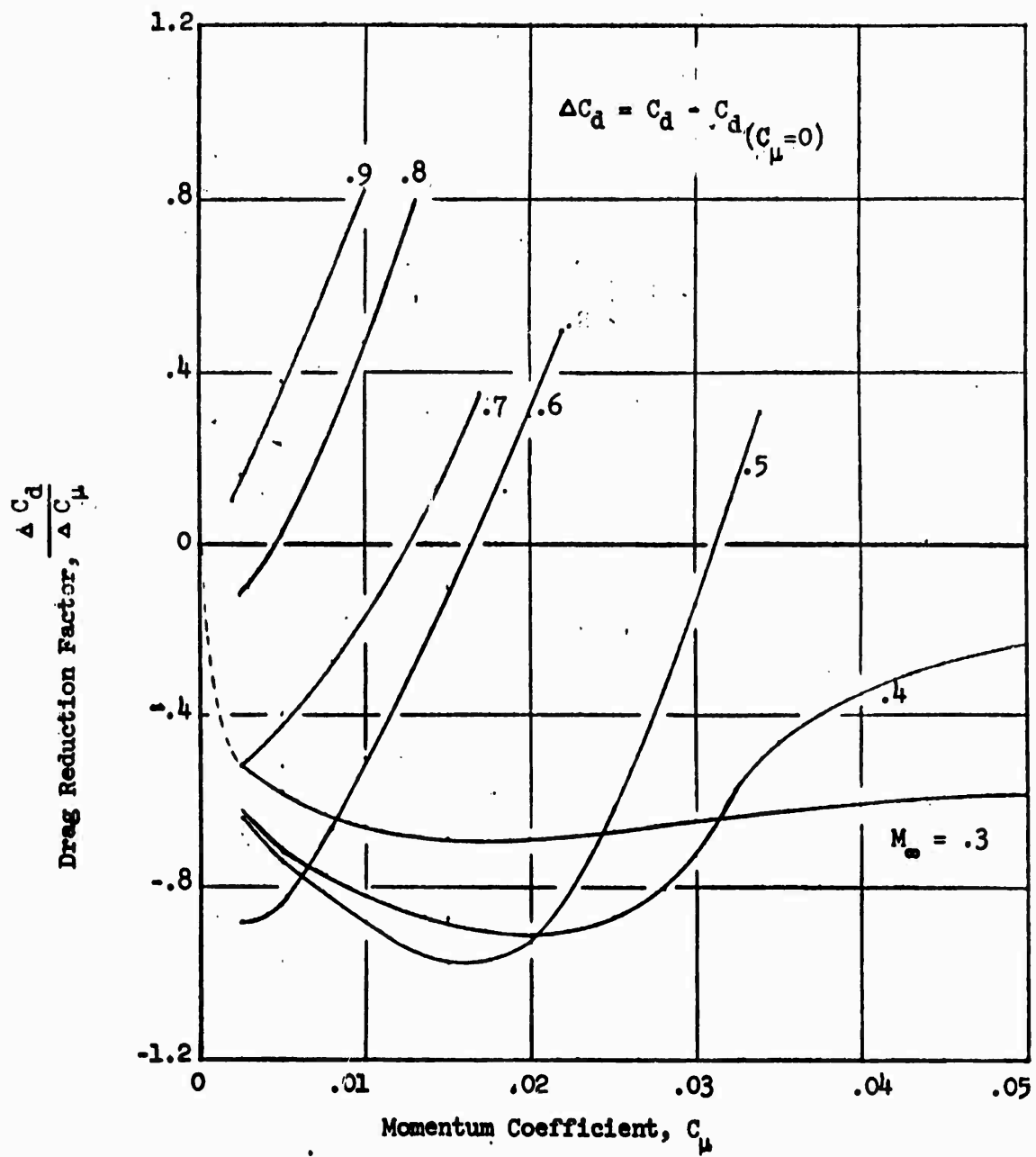
Figure 15 - Rounded Ellipse Drag Reduction

30
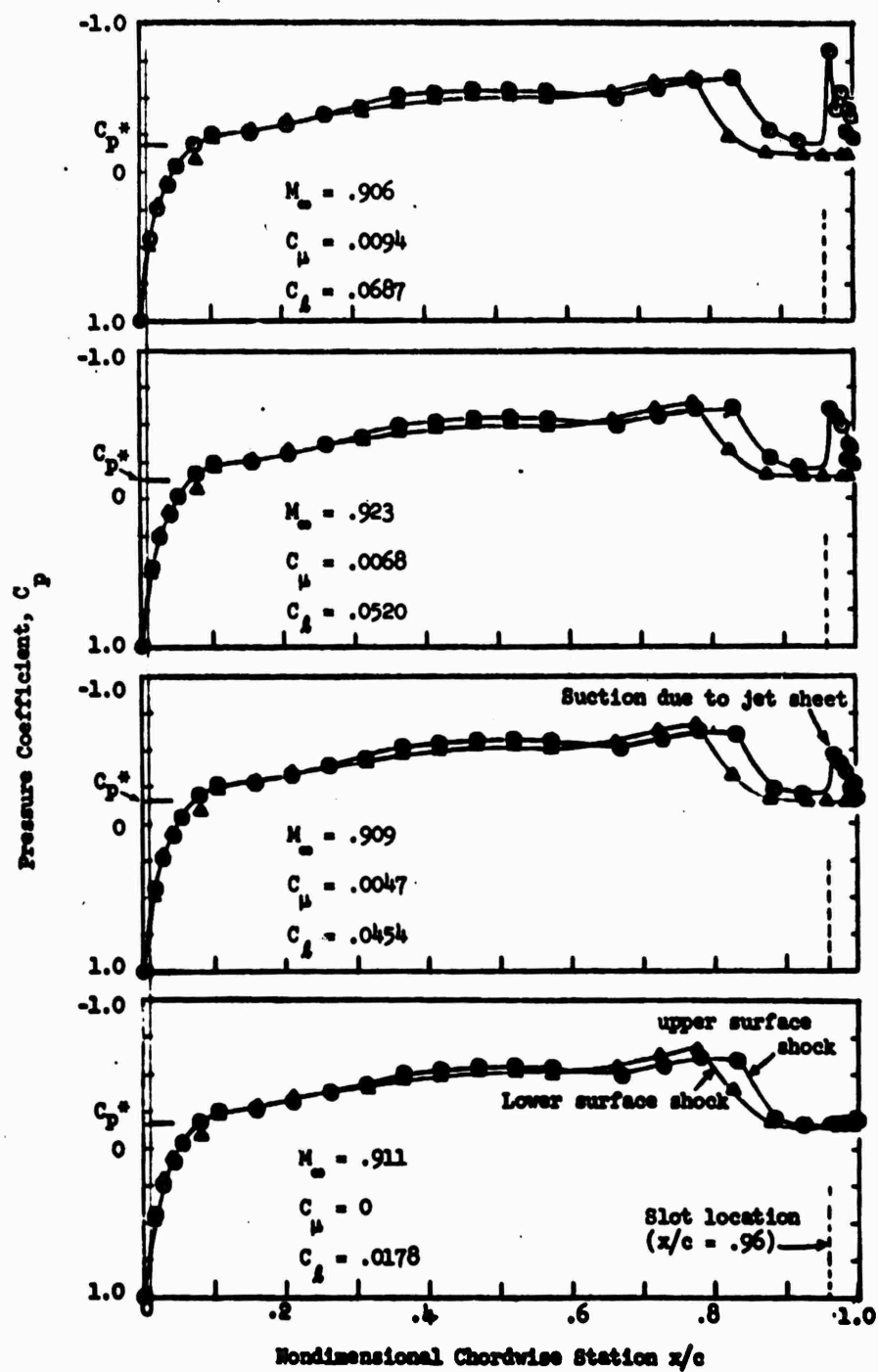
Figure 16 - Pressure Distribution for Rounded Ellipse at $M_{nominal} = 0.9$, $\alpha = -1.2°$
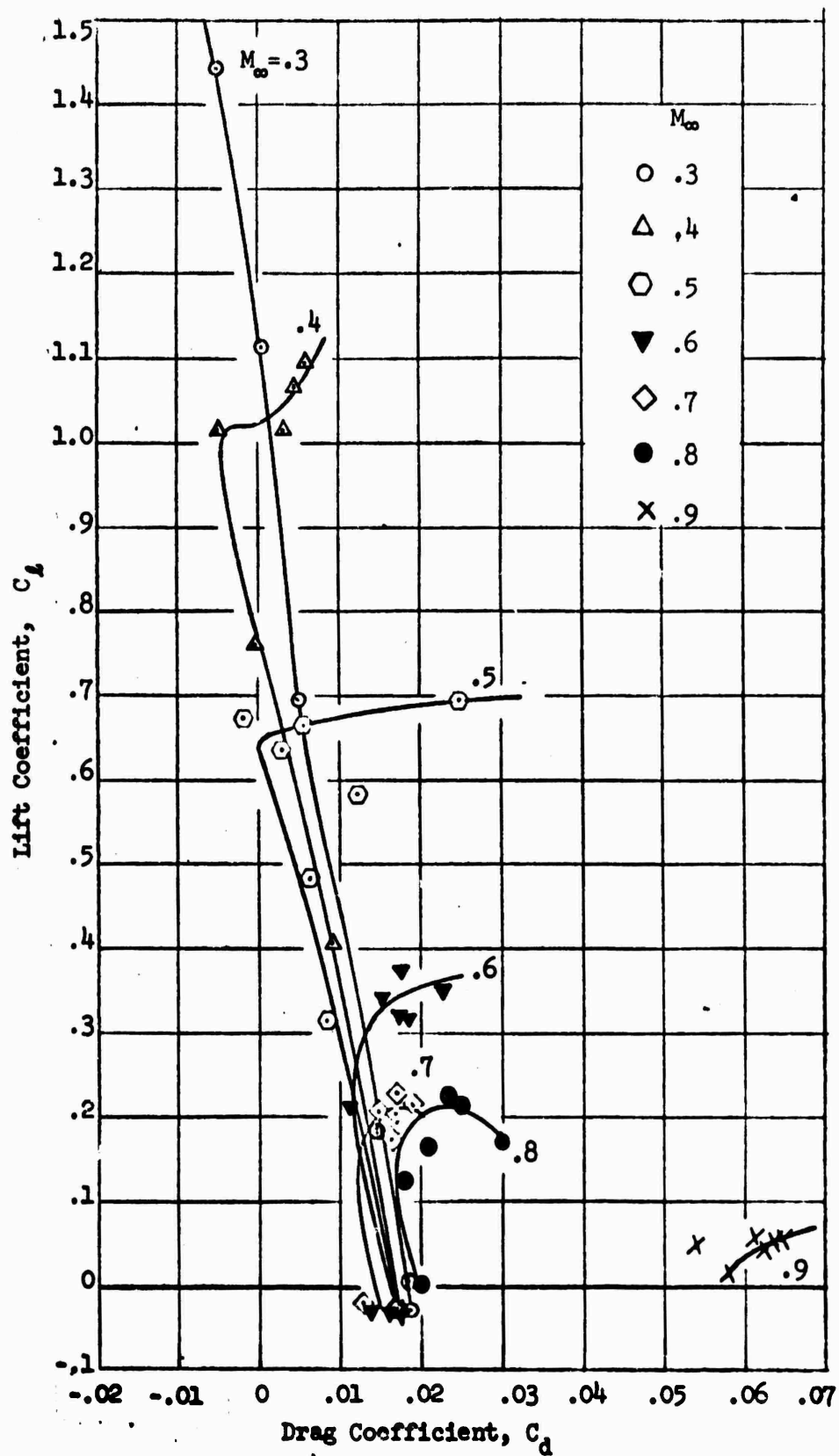
Figure 17 - Rounded Ellipse Drag Polar
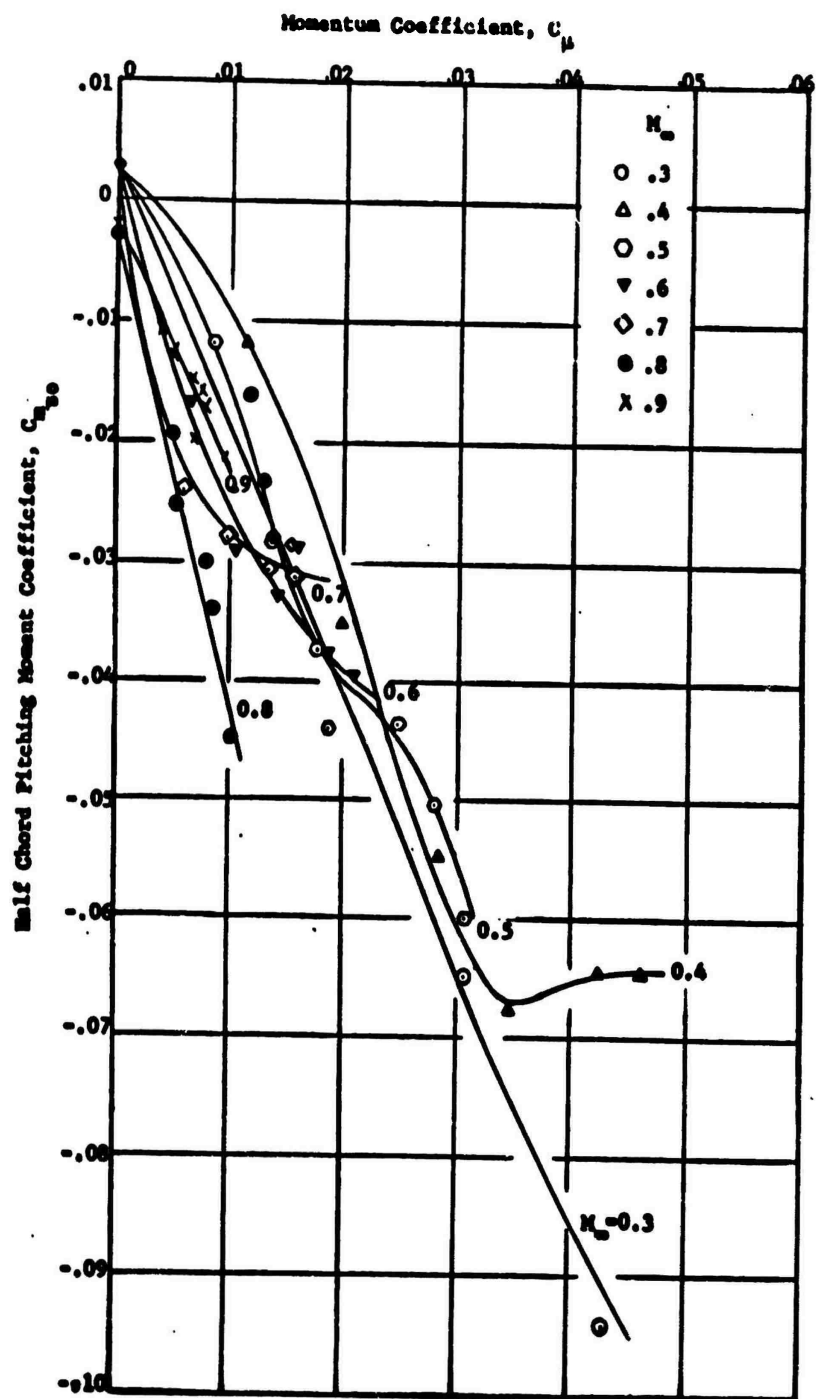
Figure 18 - Half Chord Pitching Moment
Variation for Rounded Ellipse
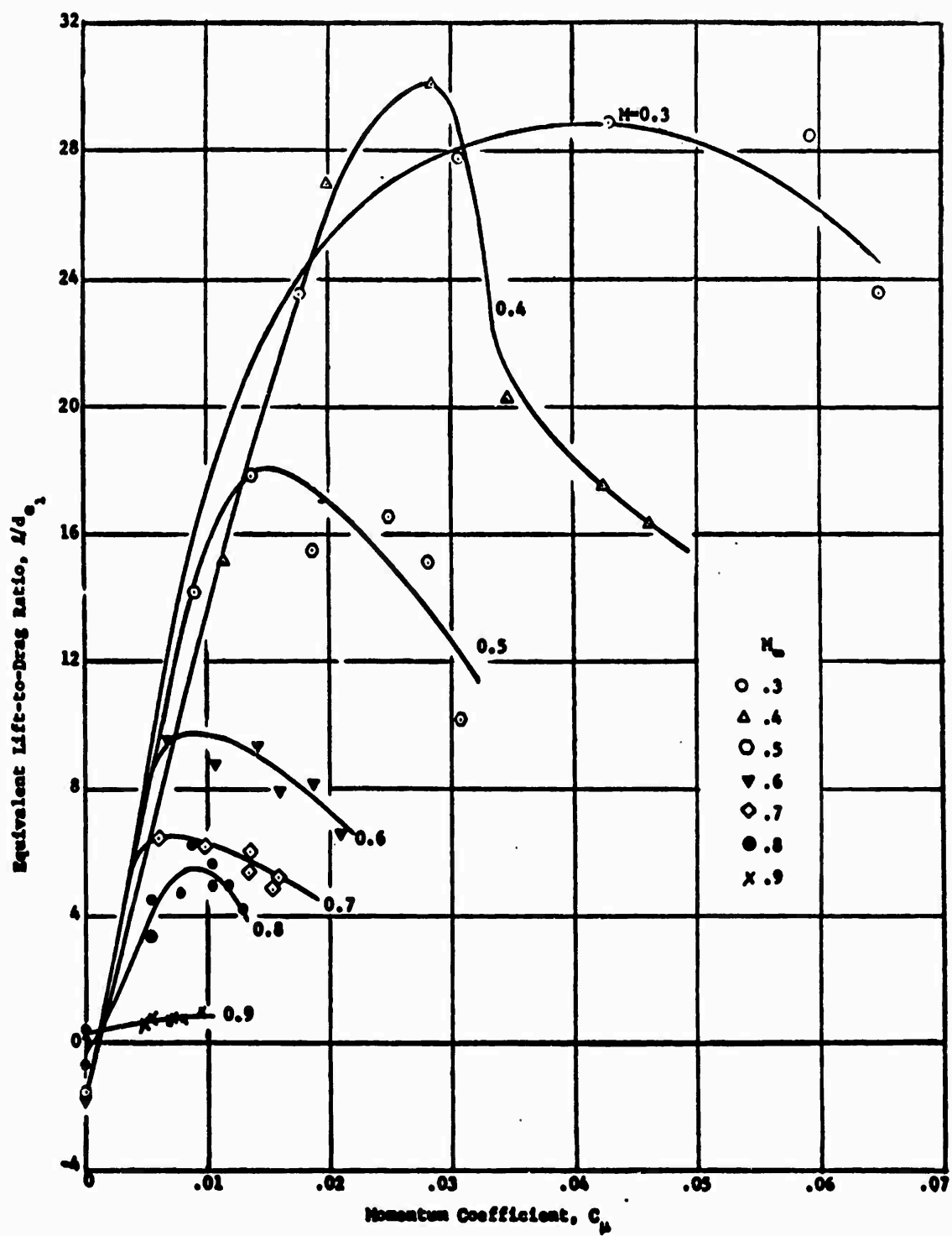
Figure 19 - Force-Based Equivalent Lift-to-Drag Ratio for Rounded Ellipse

34
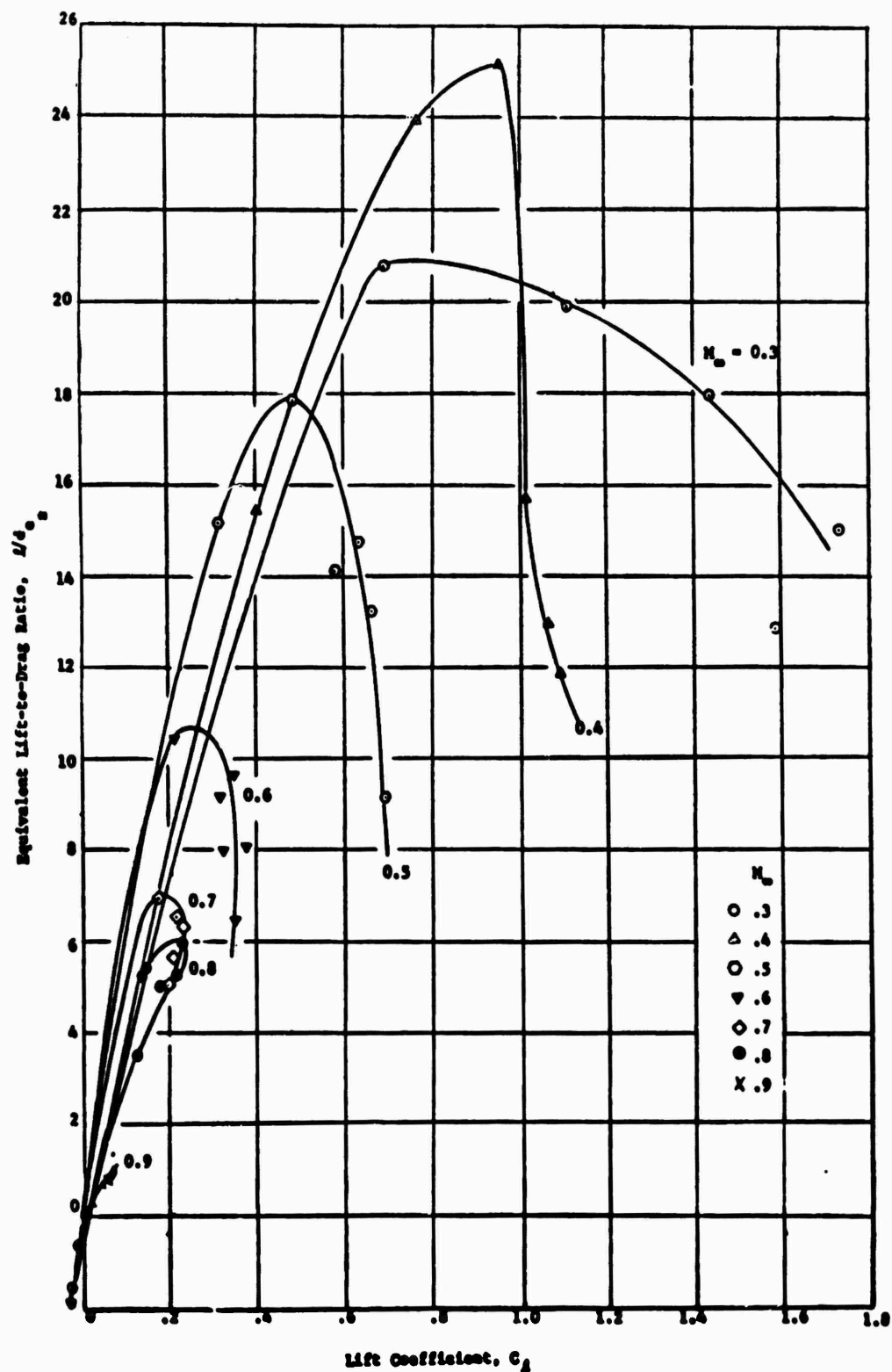
Figure 20 - Kinetic-Energy-Based Equivalent
Lift-to-Drag Ratio for Rounded Ellipse

35
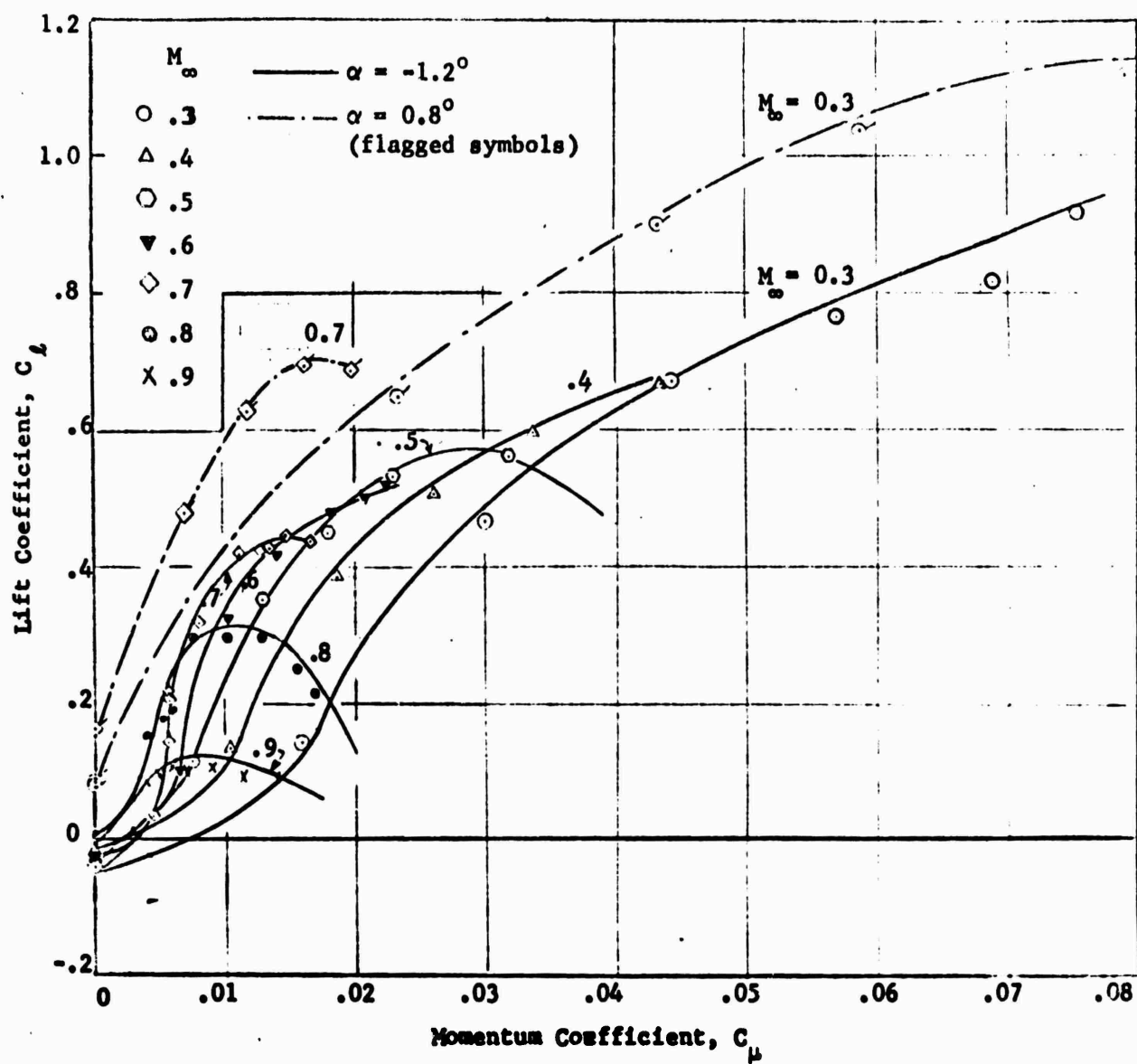
Figure 21 - Lift Variation with Momentum Coefficient for Pure Ellipse
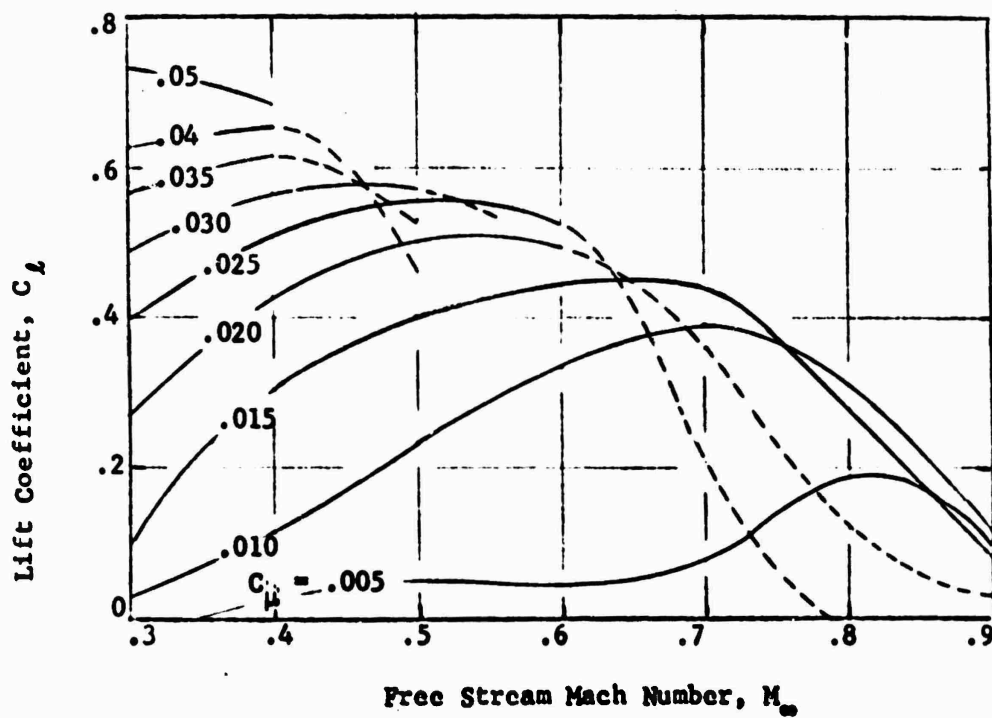
Figure 22 - Lift Variation with Mach Number
for Pure Ellipse

37
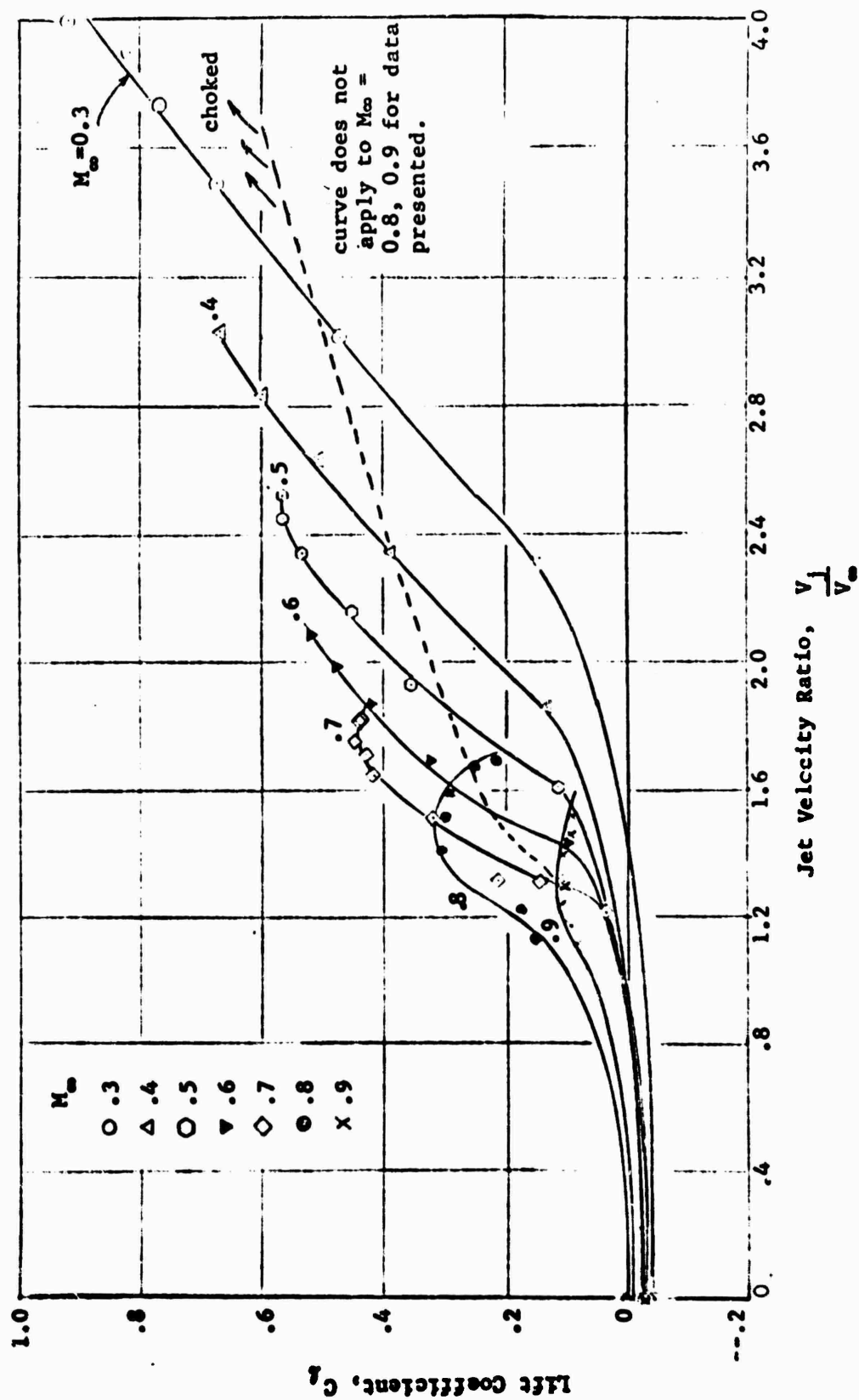
Figure 23 - Lift Variation with Jet Velocity for Pure Ellipse
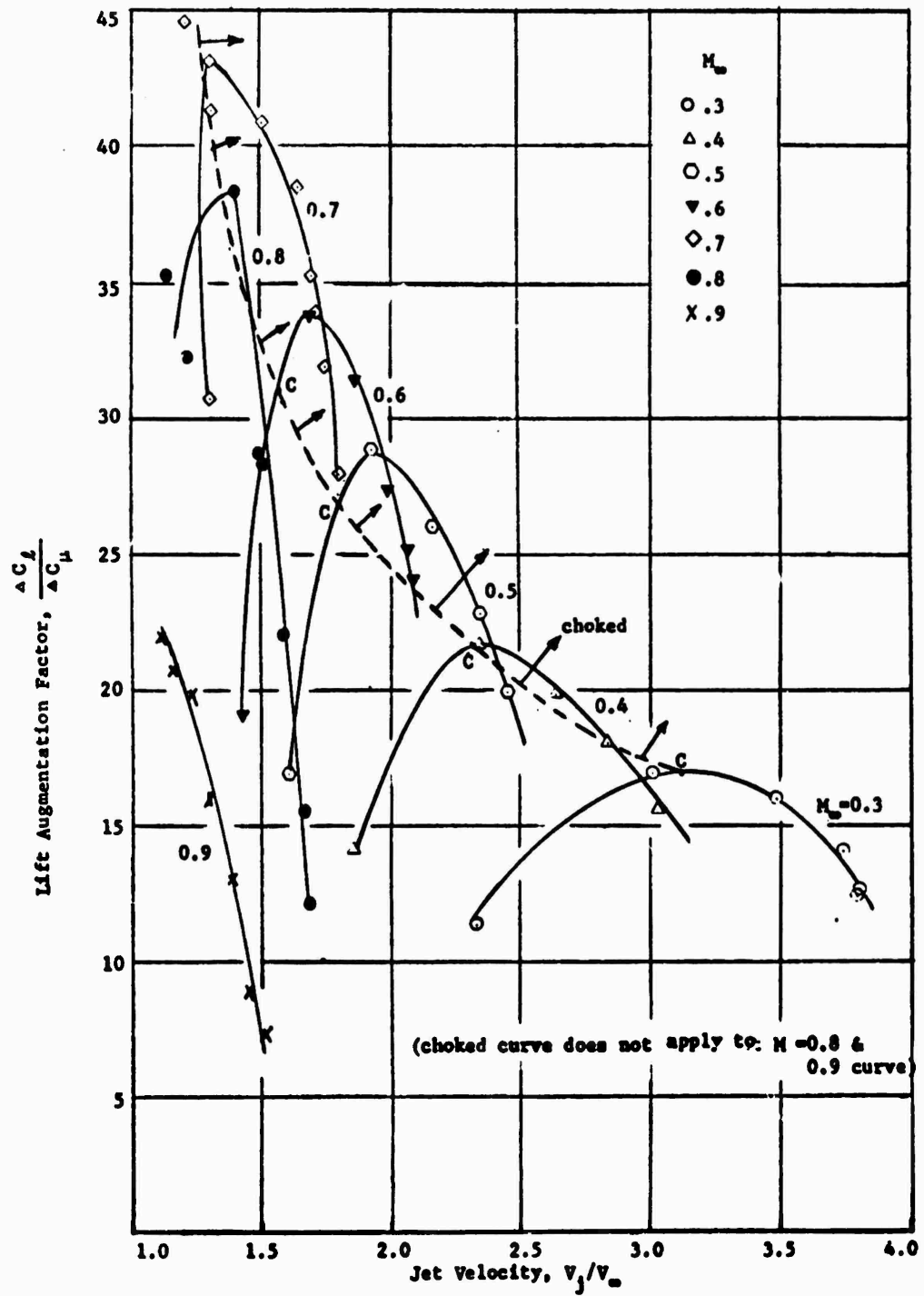
Figure 24 - Variation in Lift Augmentation with
Jet Velocity for Pure Ellipse
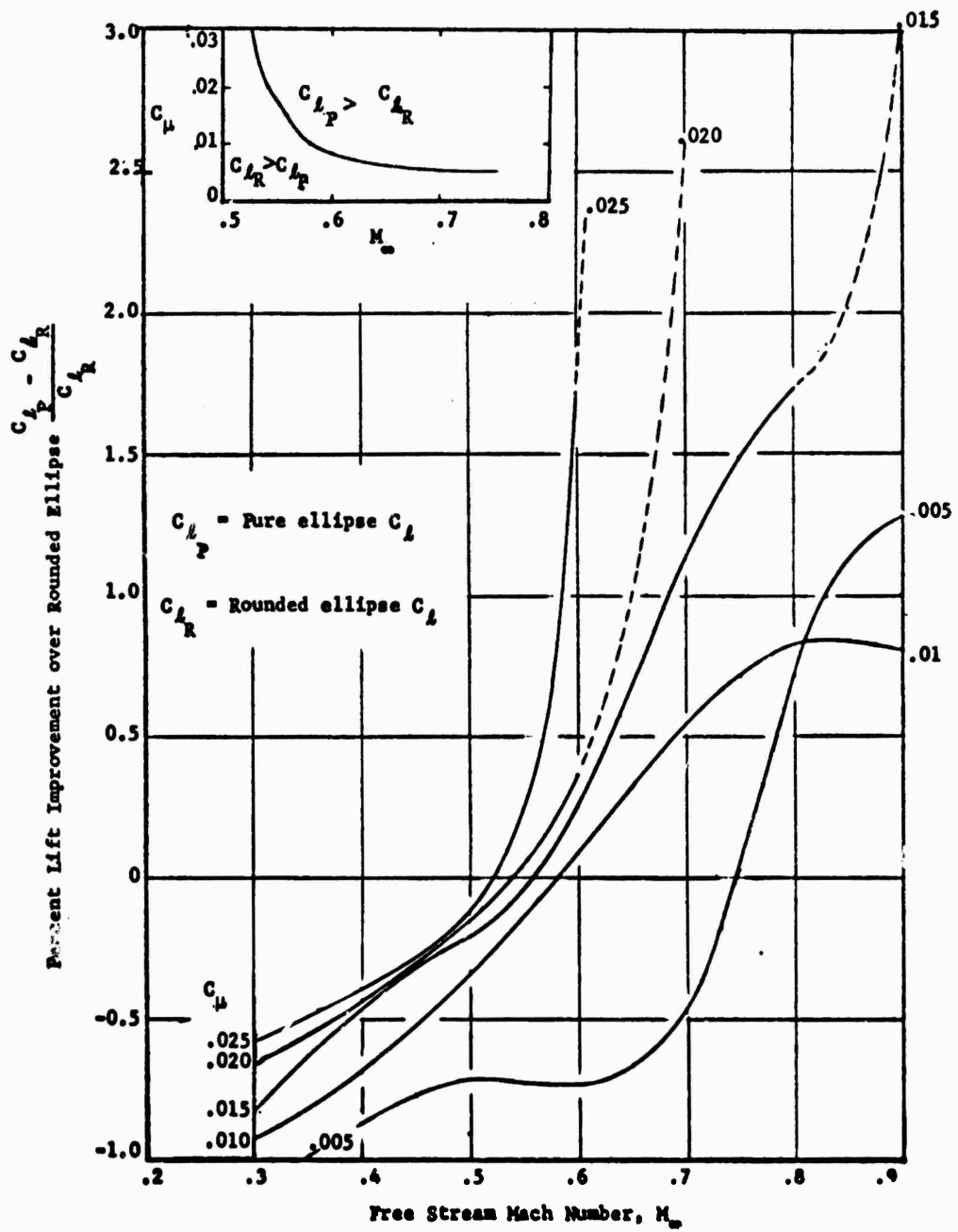
Figure 25 - Lift Comparison of Rounded
and Pure Ellipses
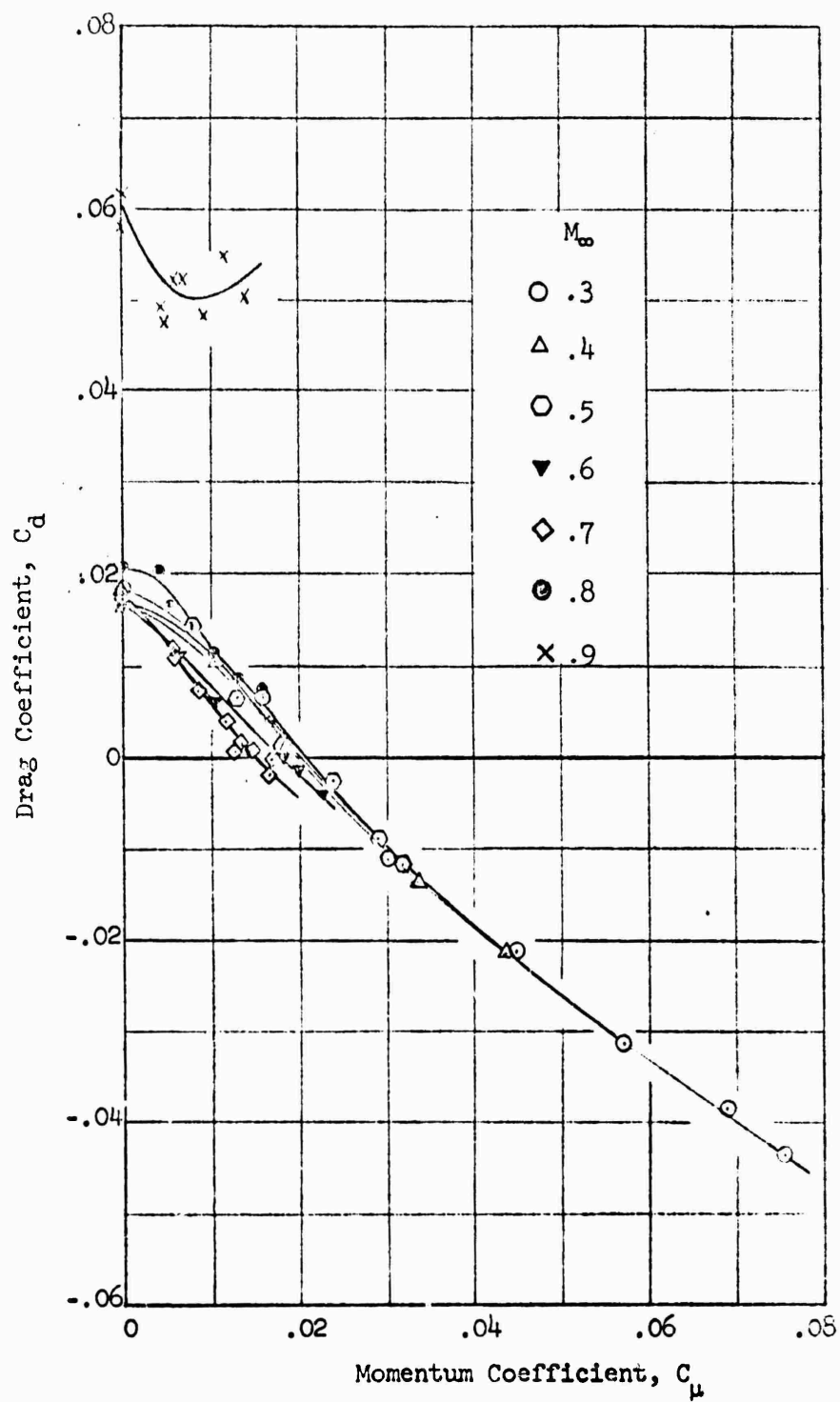
Figure 26 - Drag Variation with Momentum Coefficient for Pure Ellipse
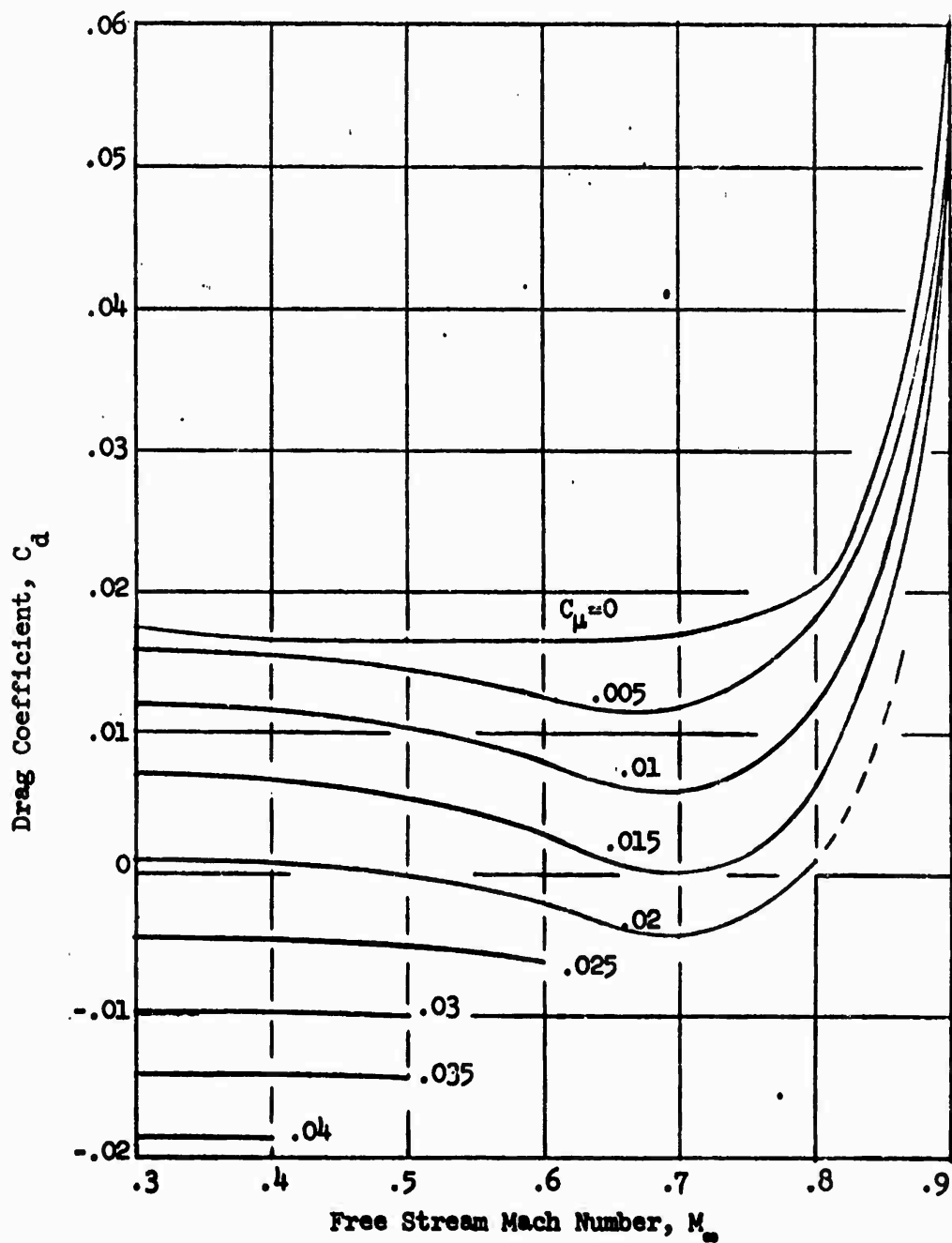
Figure 27 - Drag Variation with Mach Number for Pure Ellipse
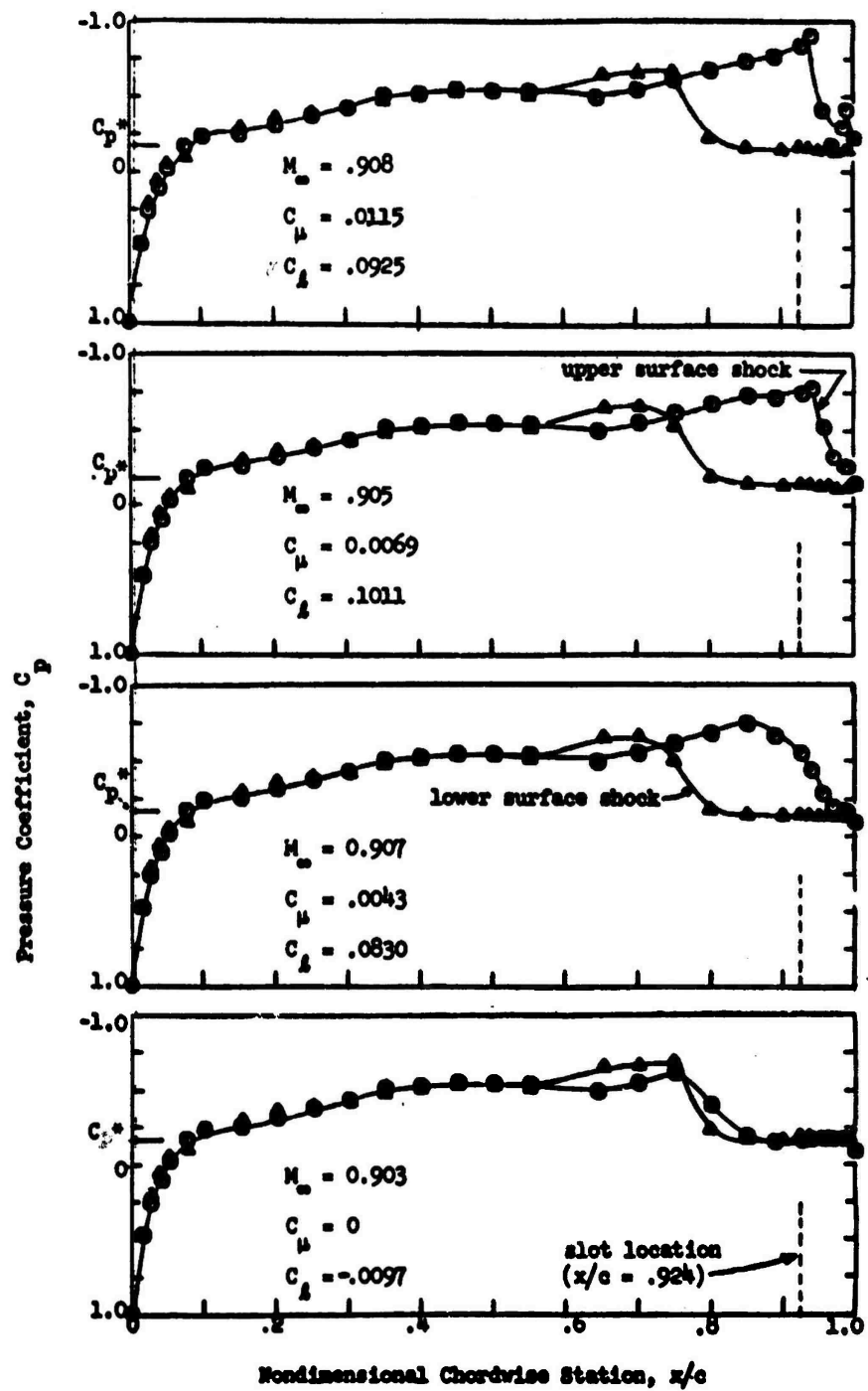
Figure 26 - Pressure Distributions for Pure Ellipse at $M_{nominal} = 0.9$
$\alpha = -1.2°$
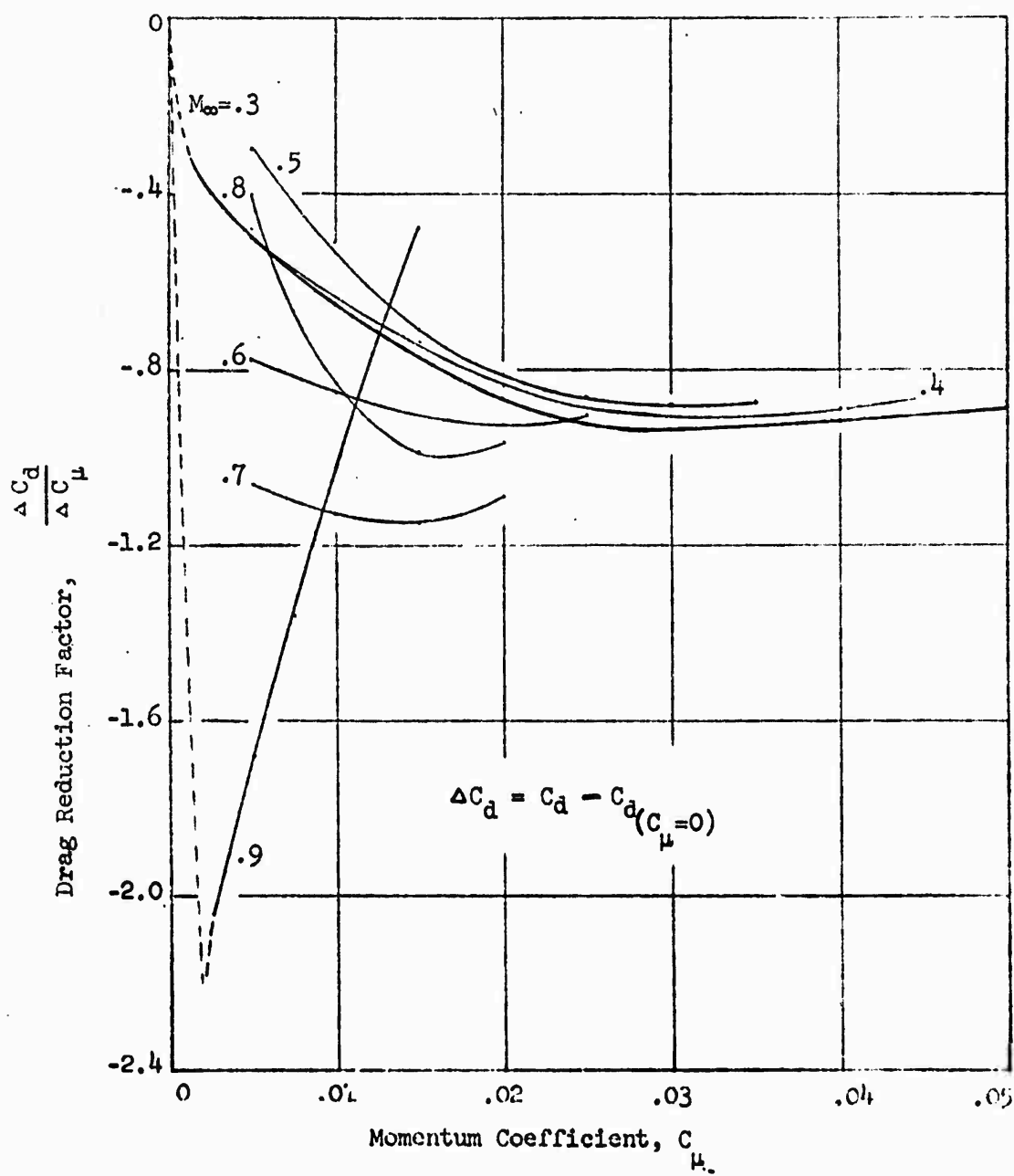
Figure 29 - Pure Ellipse Drag Reduction

44
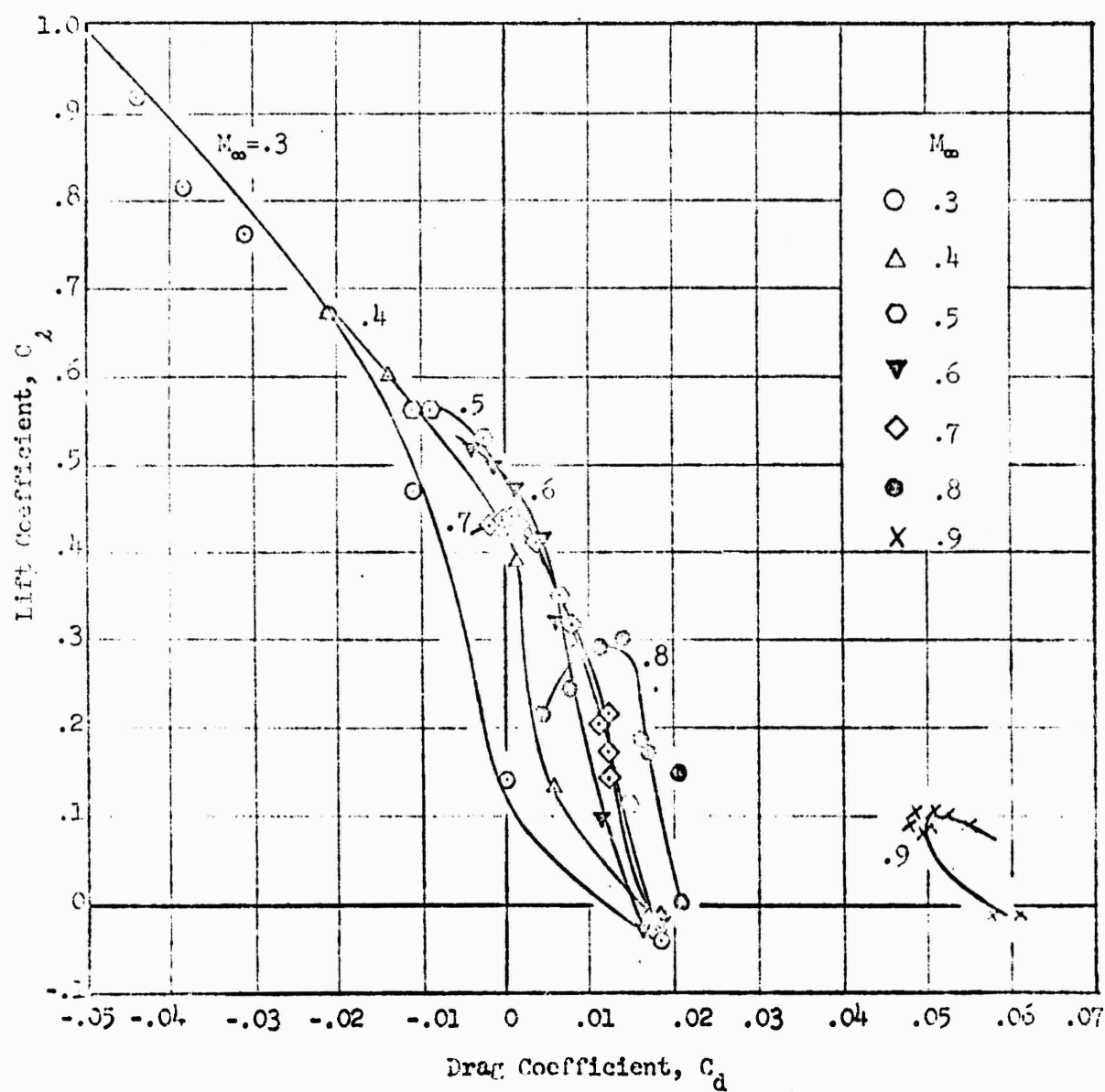
Figure 30 - Pure Ellipse Drag Polar
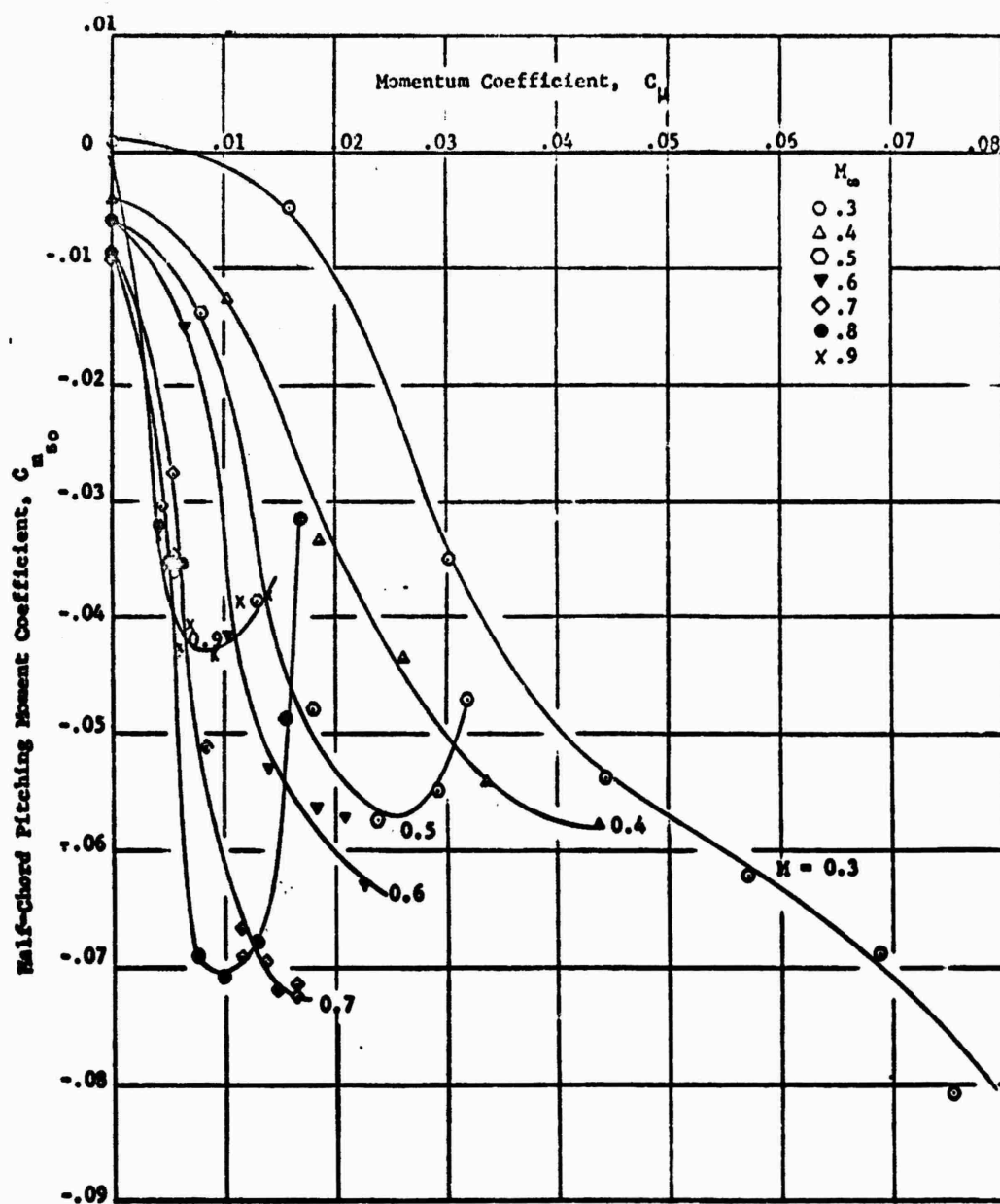
**Figure 31 - Variation in Pitching Moment with Momentum
Coefficient for Pure Ellipse**

46
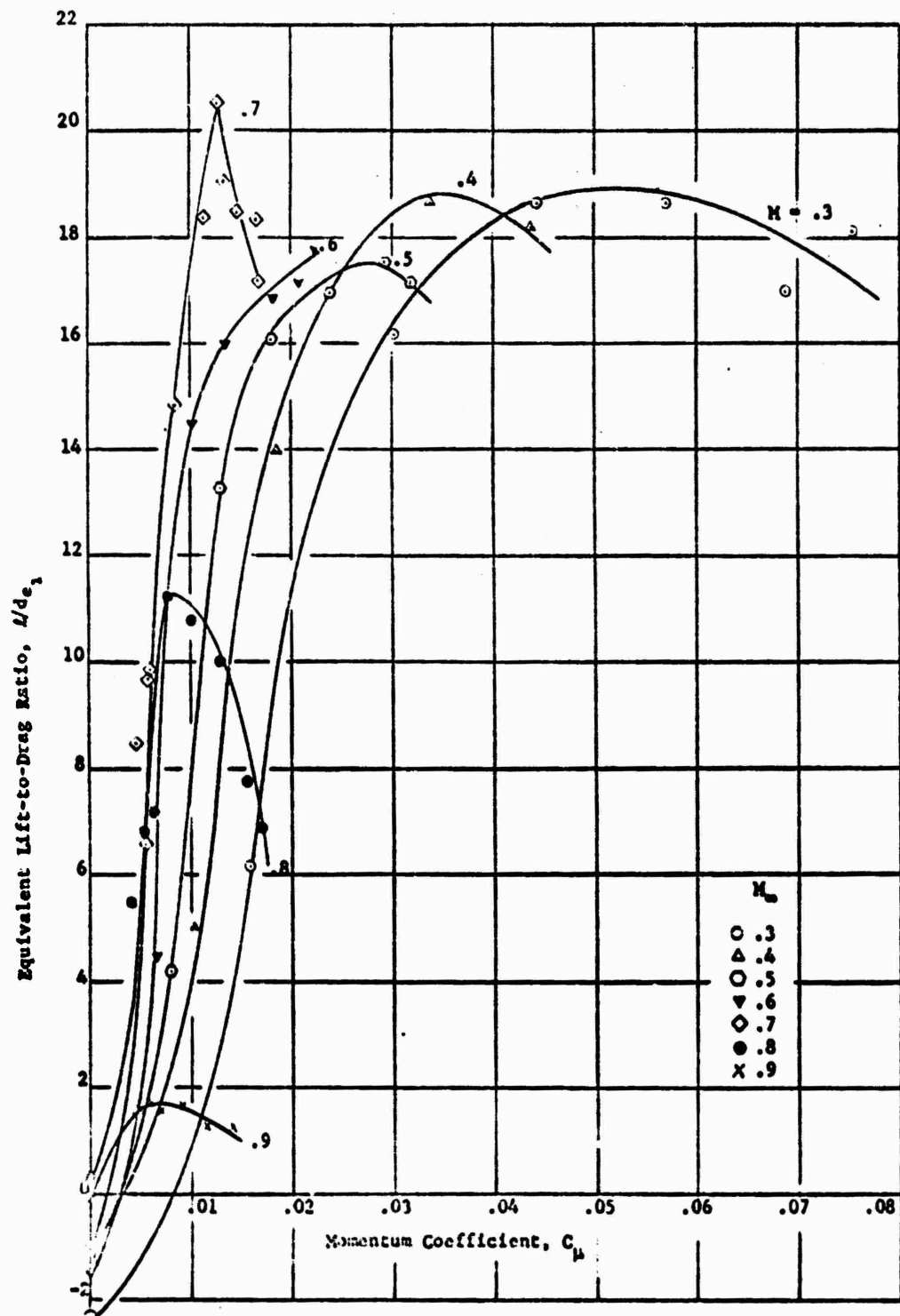
Figure 32 - Force-Based Equivalent Lift-to-Drag
Ratio For Pure Ellipse

47

Figure 33 - Kinetic-Energy-Based Equivalent
Lift-to-Drag Ratio For Pure Ellipse
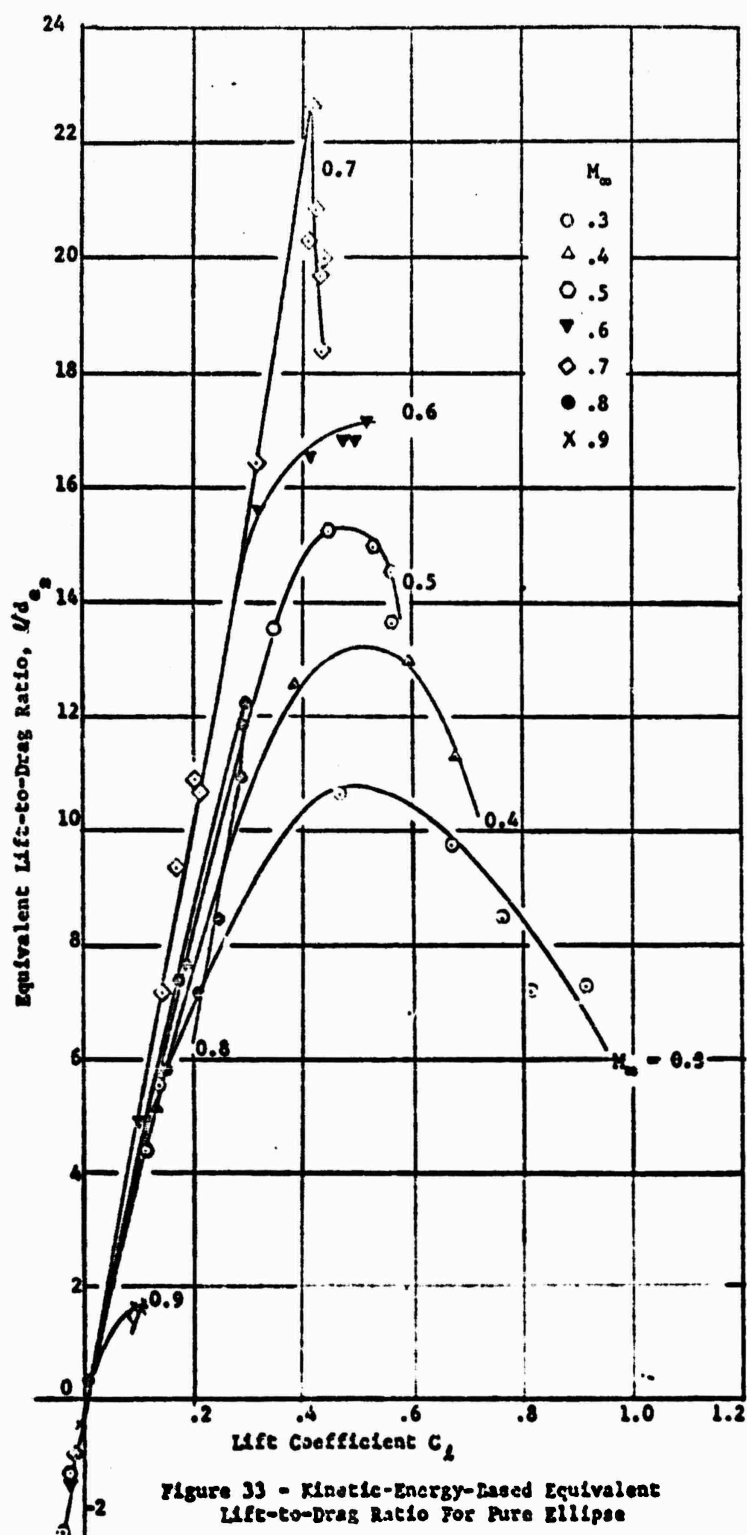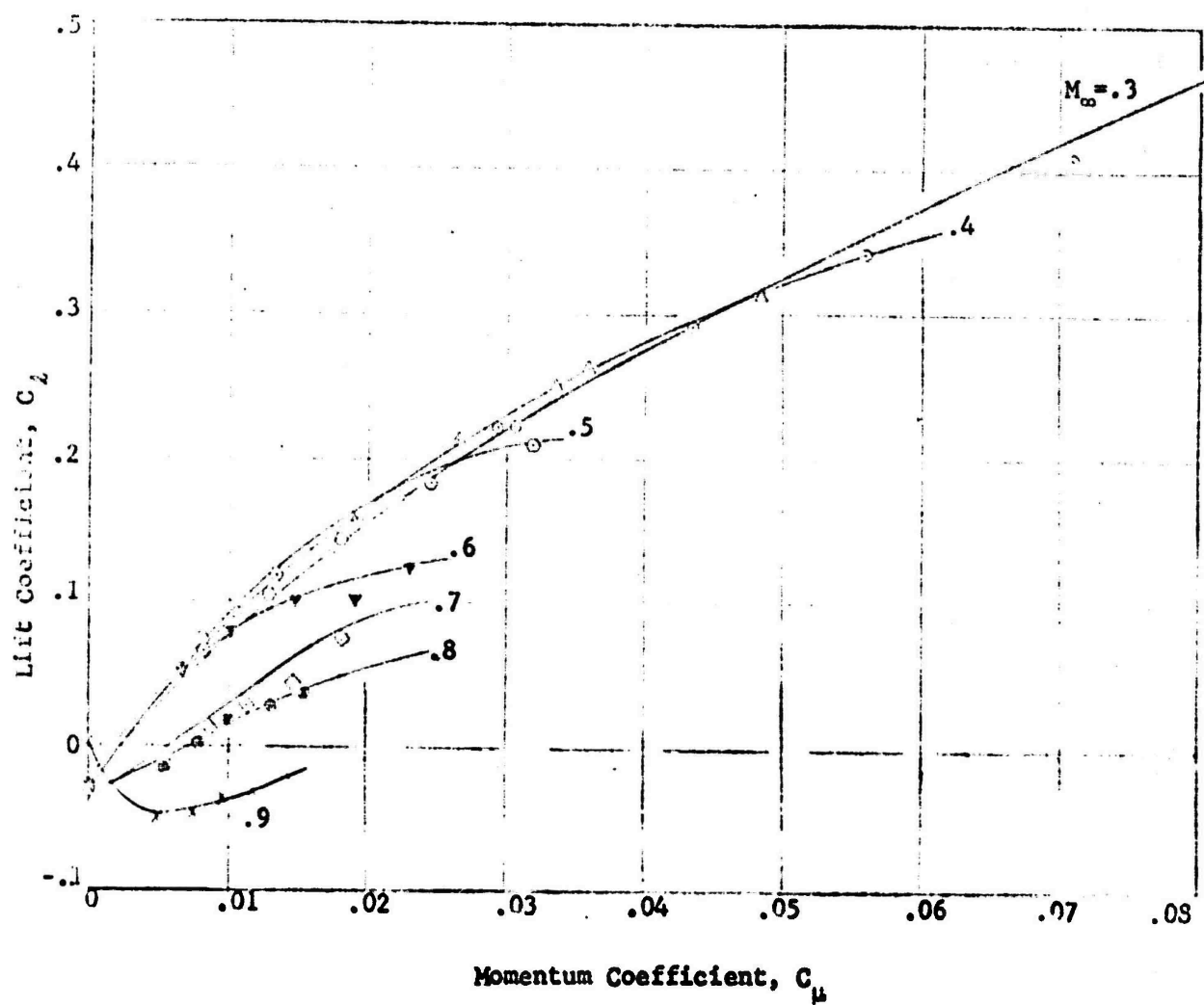
Figure 34 - Jet Flap Lift Variation with Momentum Coefficient
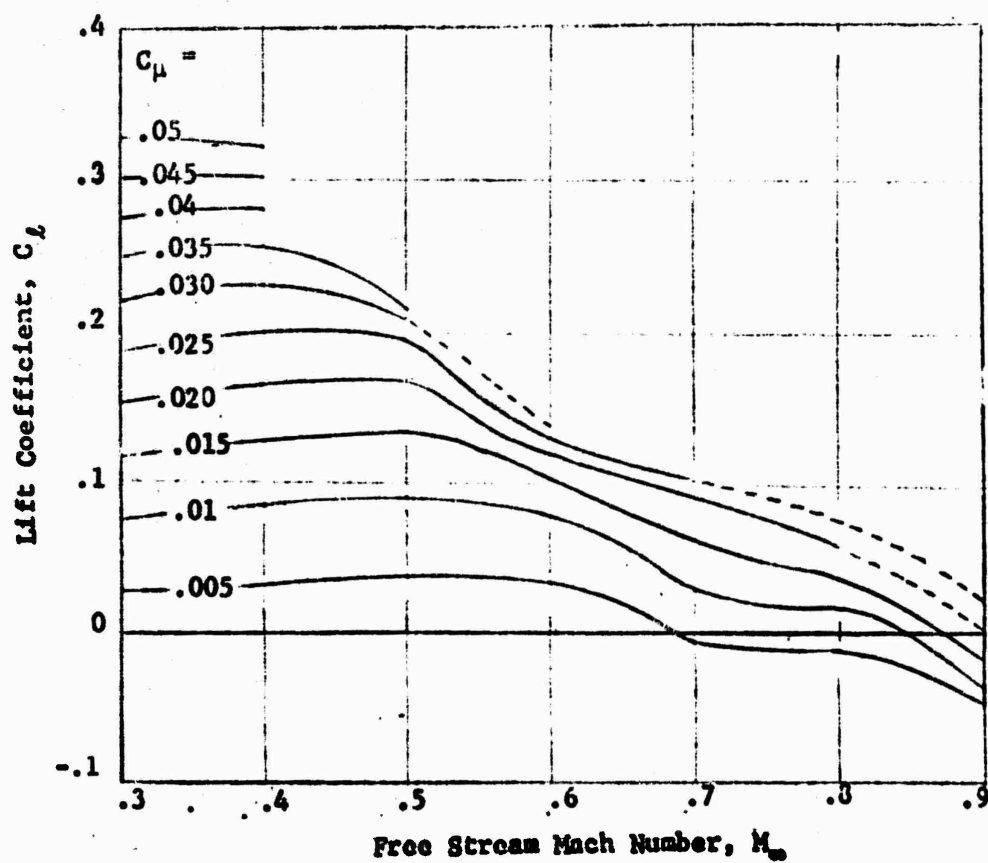
Figure 35 - Jet Flap Lift Variation with Mach Number
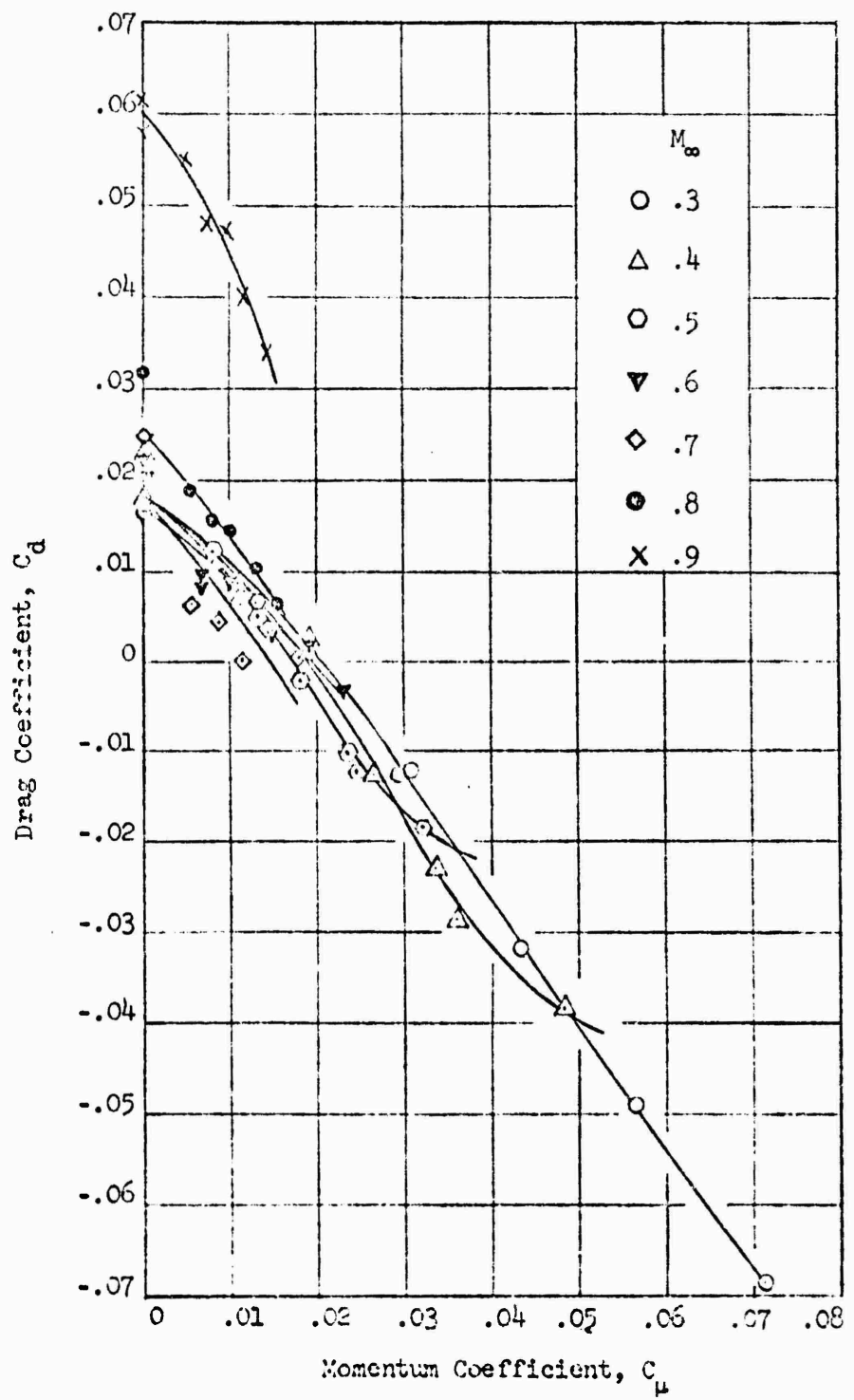
Figure 36 - Drag Variation with Momentum Coefficient for Jet Flap

51
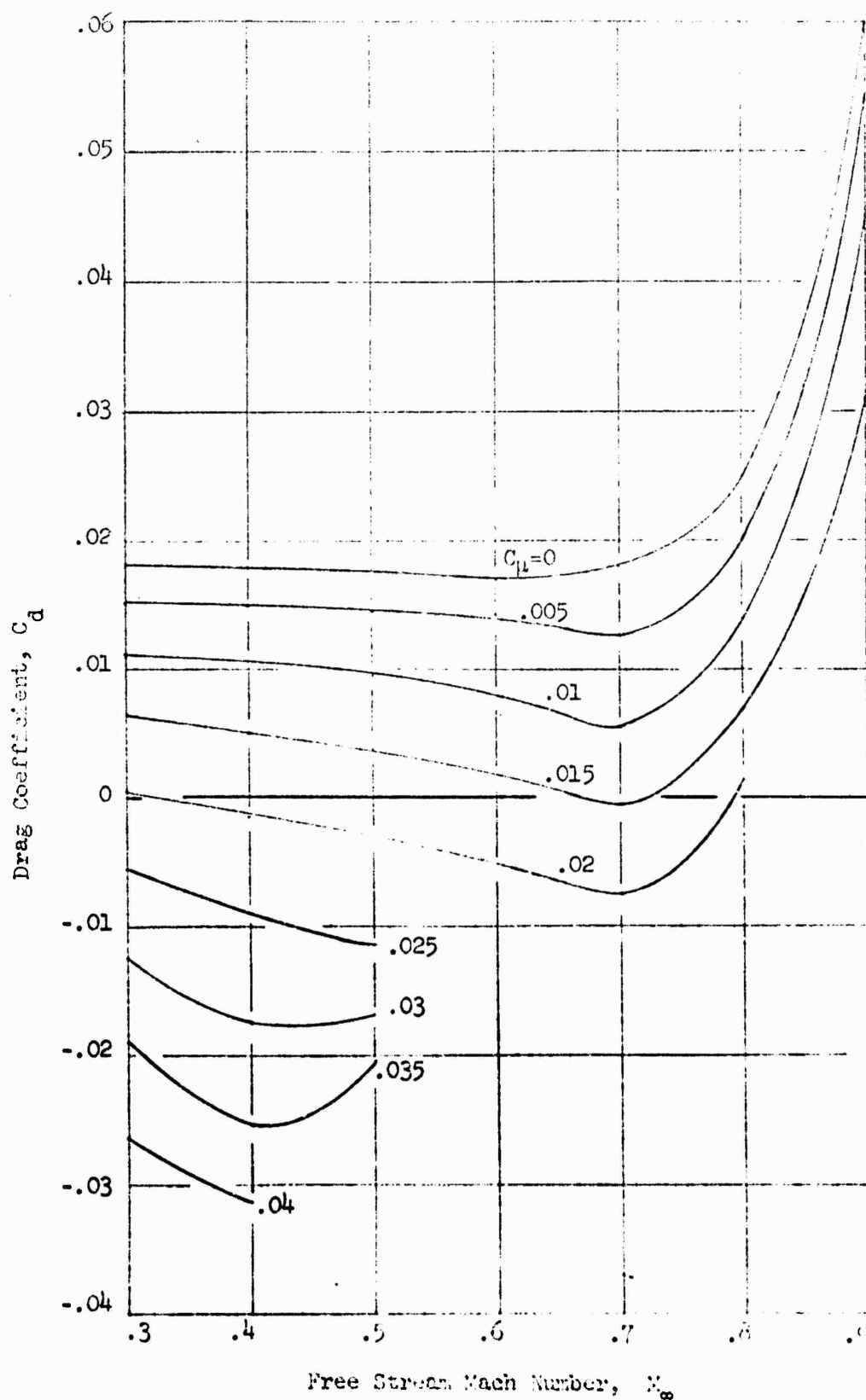
Figure 37 - Jet Flap Drag Variation with Mach Number
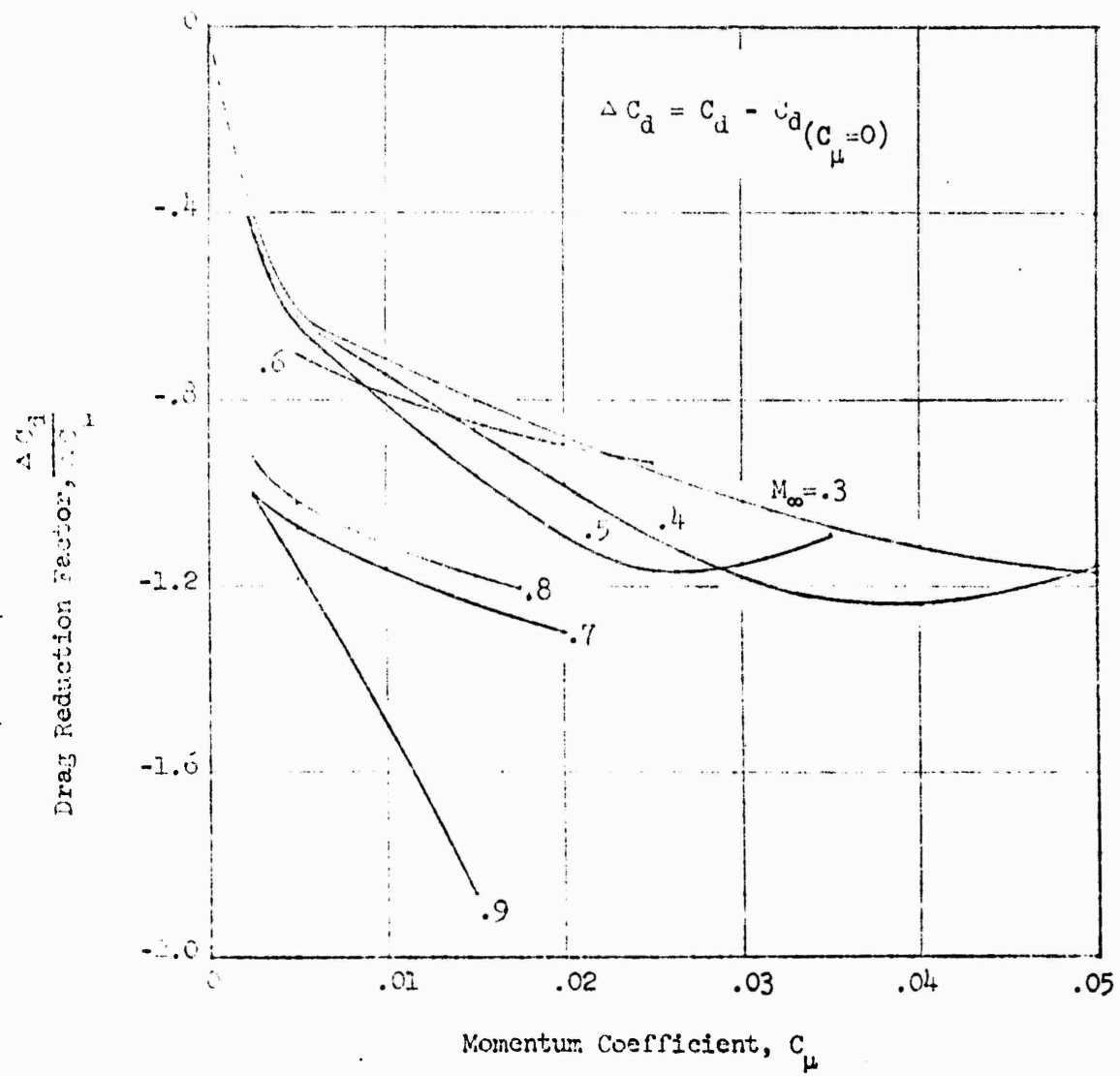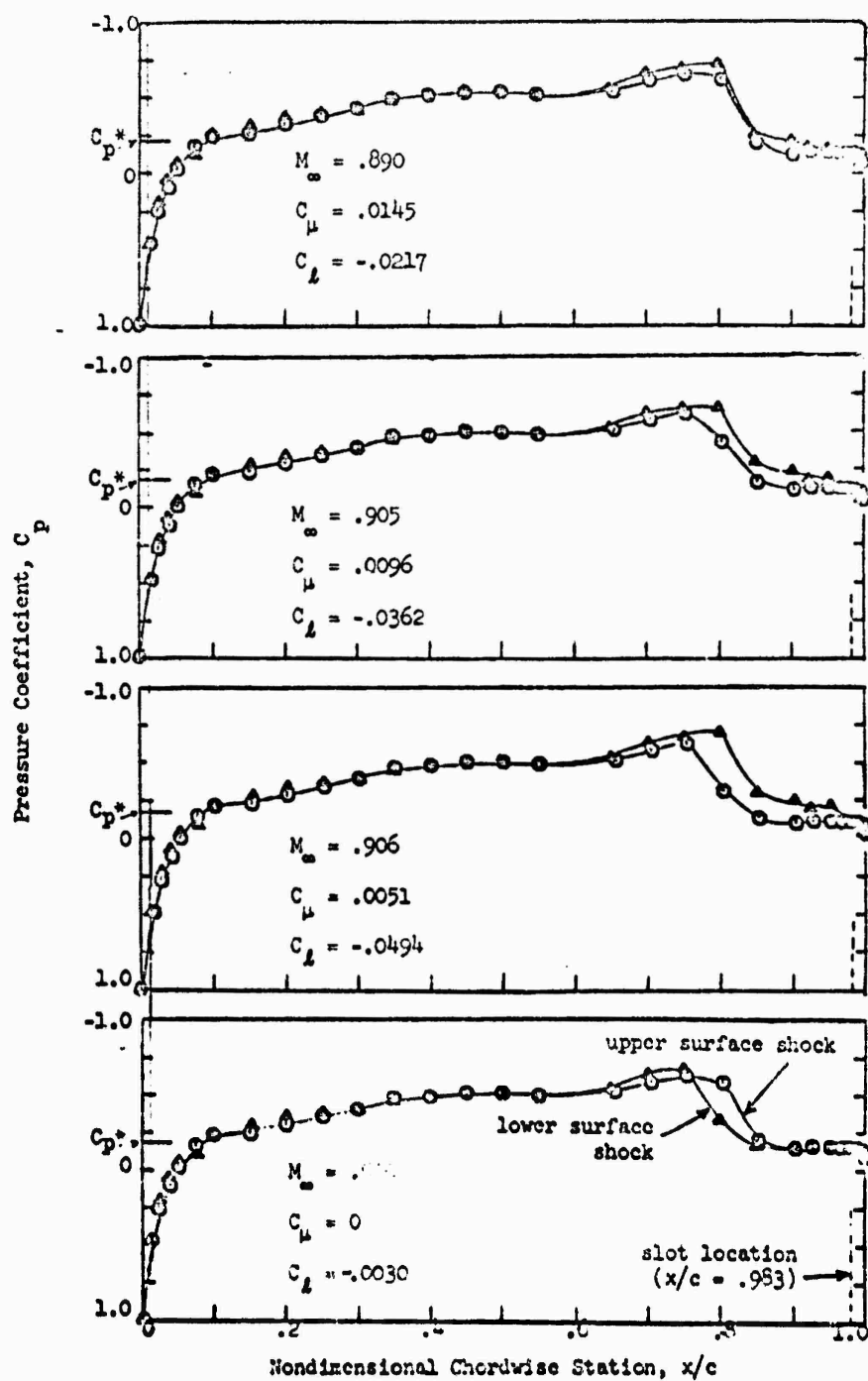
Figure 38 - Jet Flap Drag Reduction

53

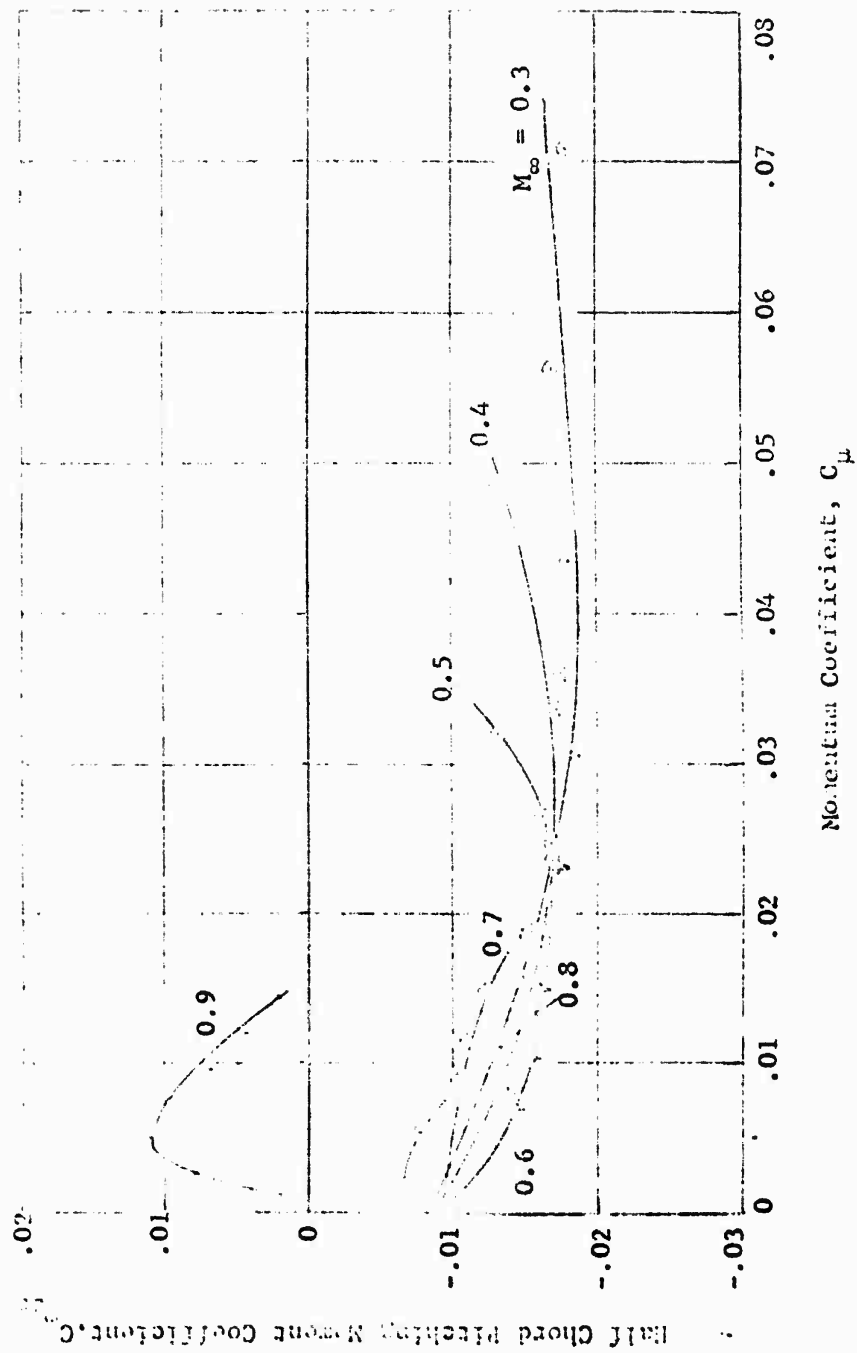Figure 39 - Pressure Distributions for Jet Flap at $M_{nominal} = 0.9$, $\alpha = -1.2°$

54

Figure 40 - Half Chord Pitching Moment Variation
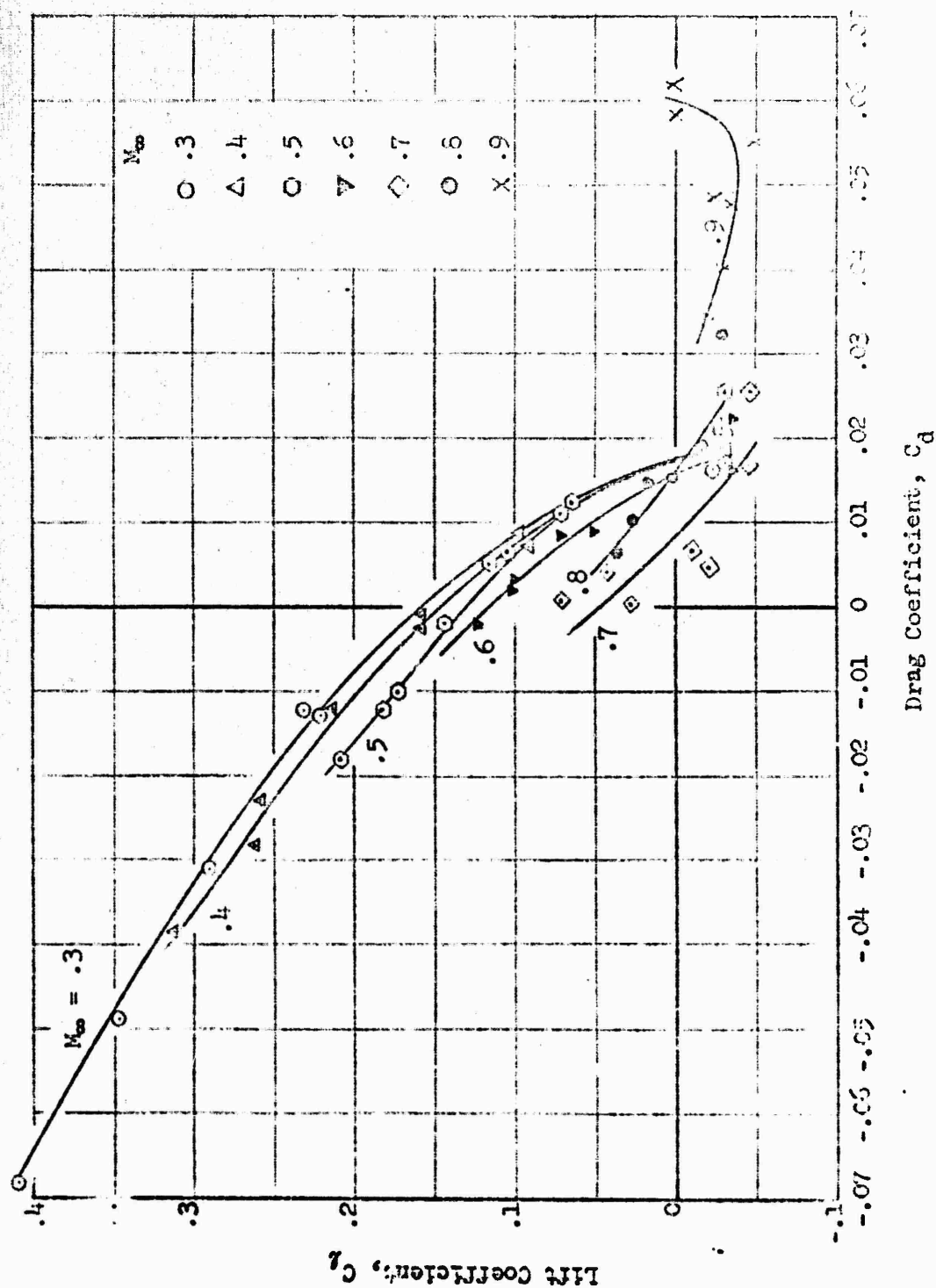With Momentum Coefficient for Jet Flap
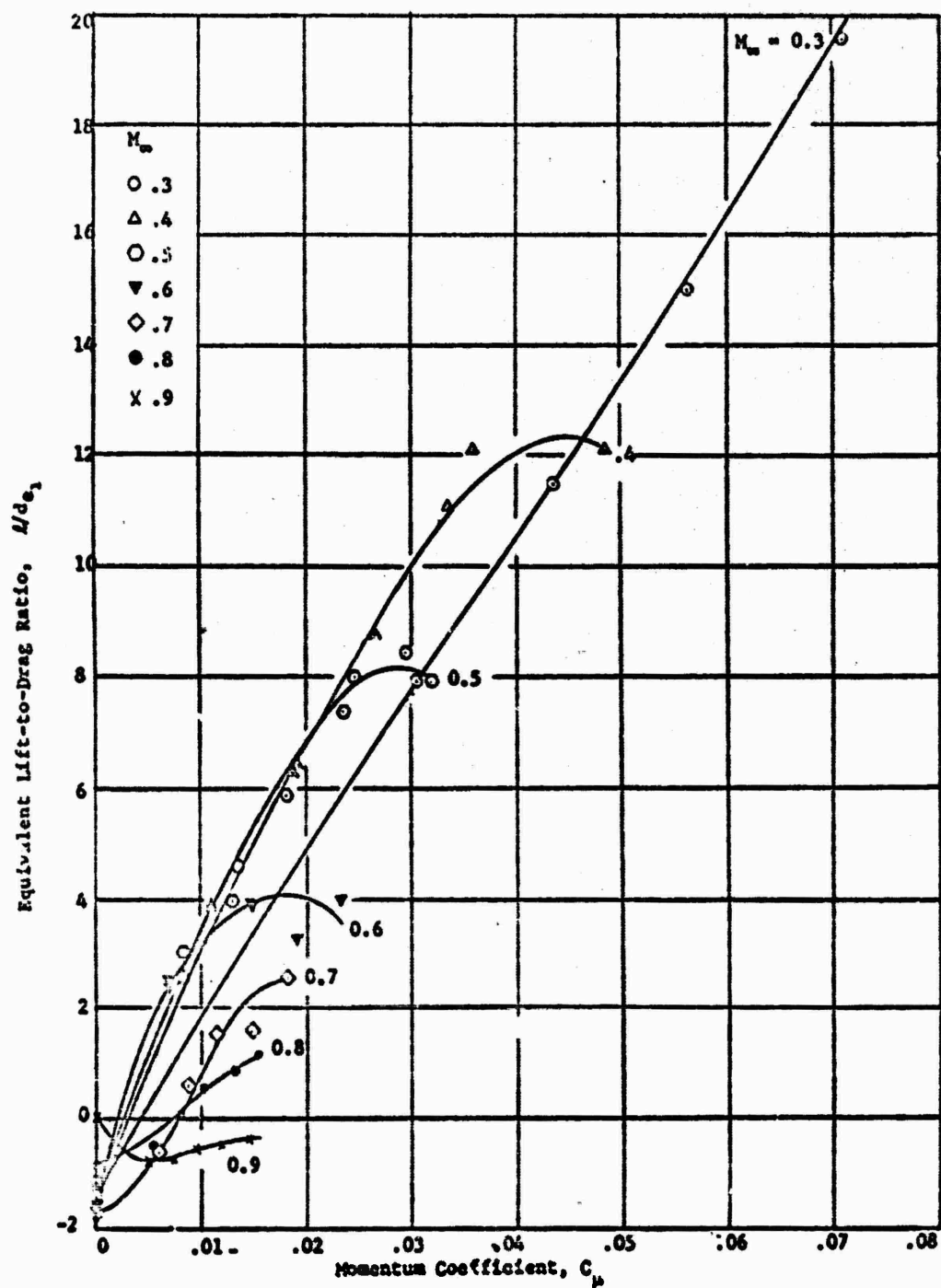
Figure 41 - Jet Flap Drag Polar

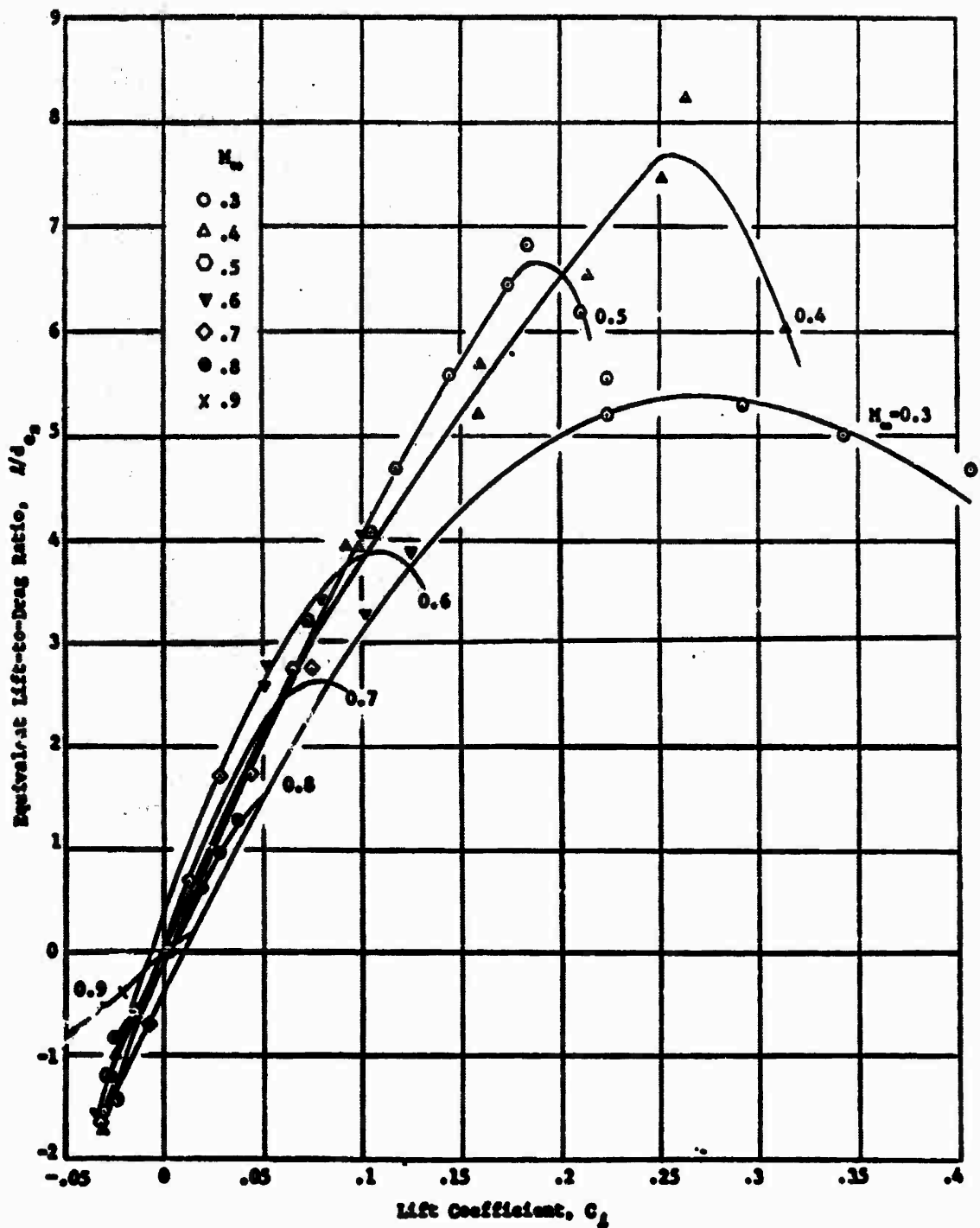Figure 42 - Force-Based Equivalent Lift-to-Drag Ratio For Jet Flap

Figure 43 - Kinetic-Energy-Based Equivalent Lift-to-Drag Ratio for Jet Flap
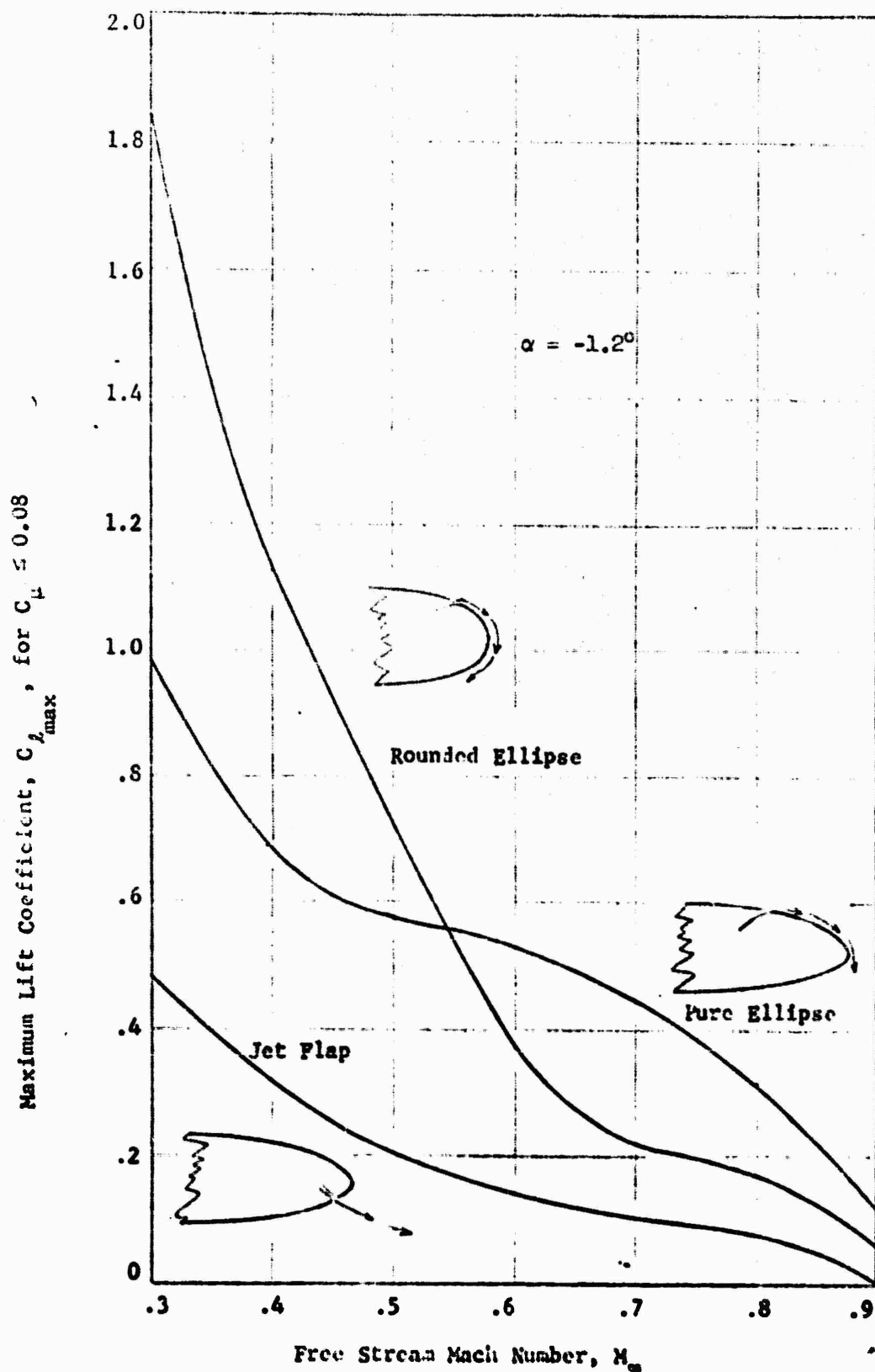
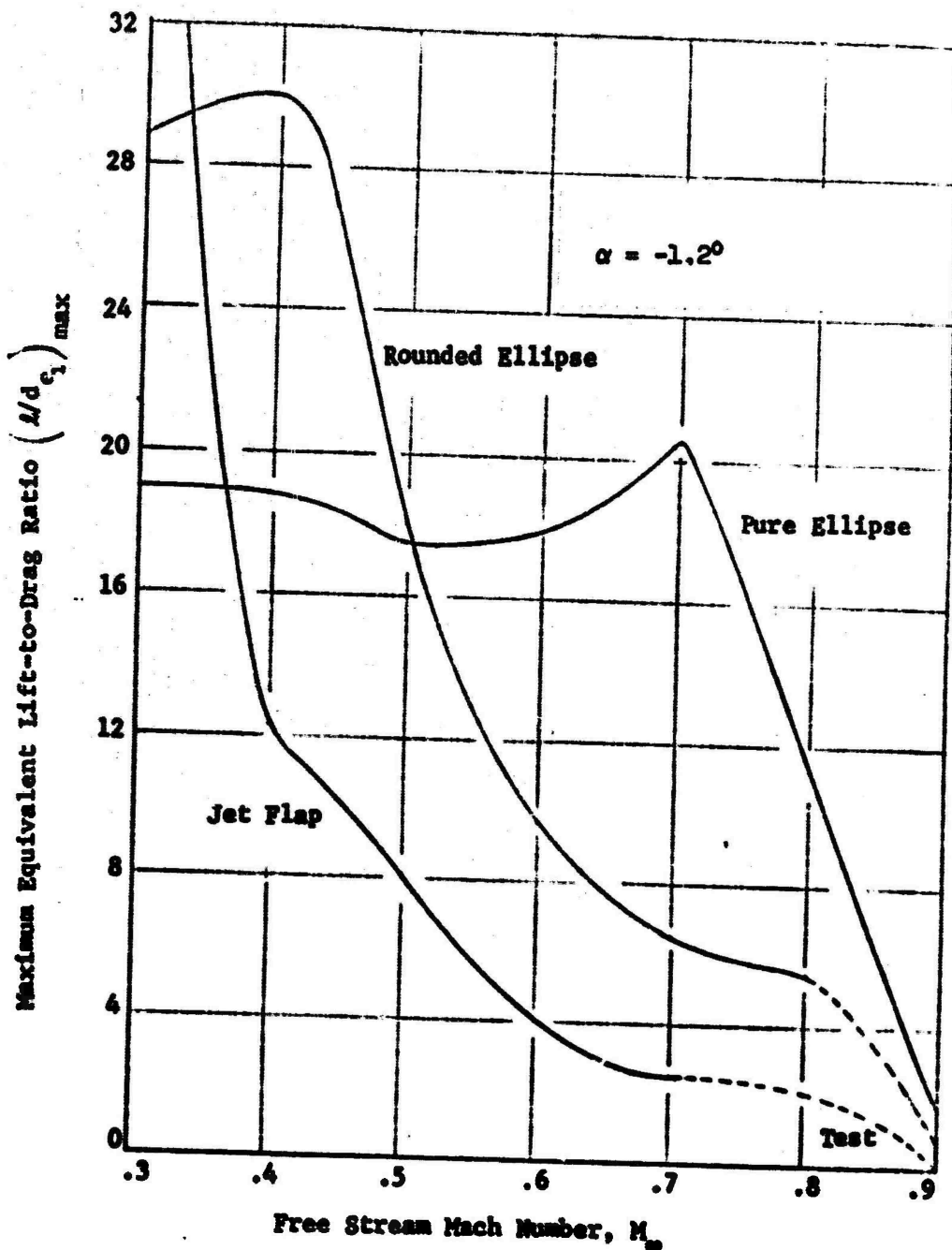Figure 44 - Comparative Lift Characteristics
of The Three Models

Figure 45 - Comparison of Maximum Force-Based
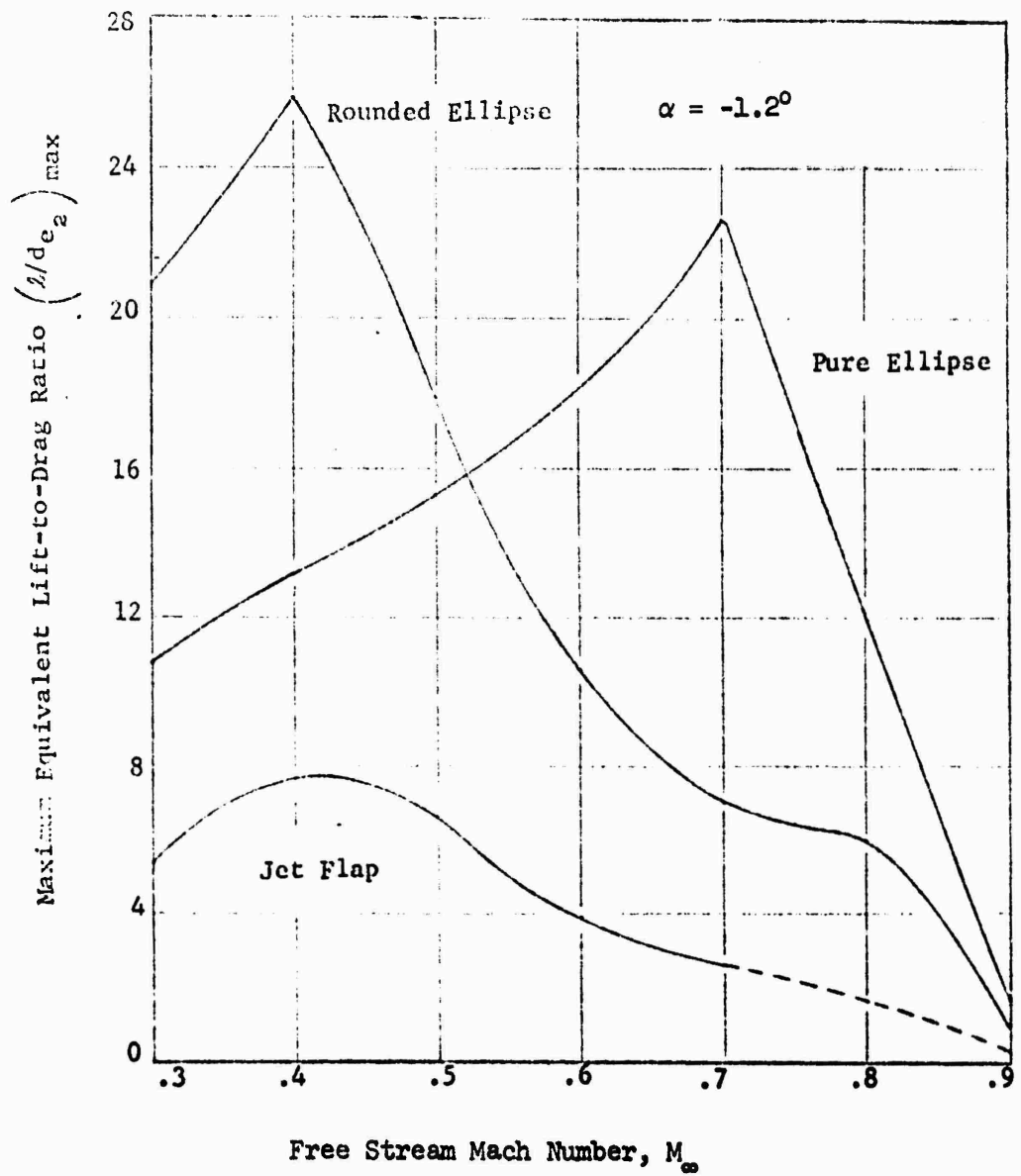Equivalent Lift-to-Drag Ratio for the
Three Configurations

Figure 46 - Comparison of Maximum Kinetic-Energy-Based
Equivalent Lift-to-Drag Ratio For
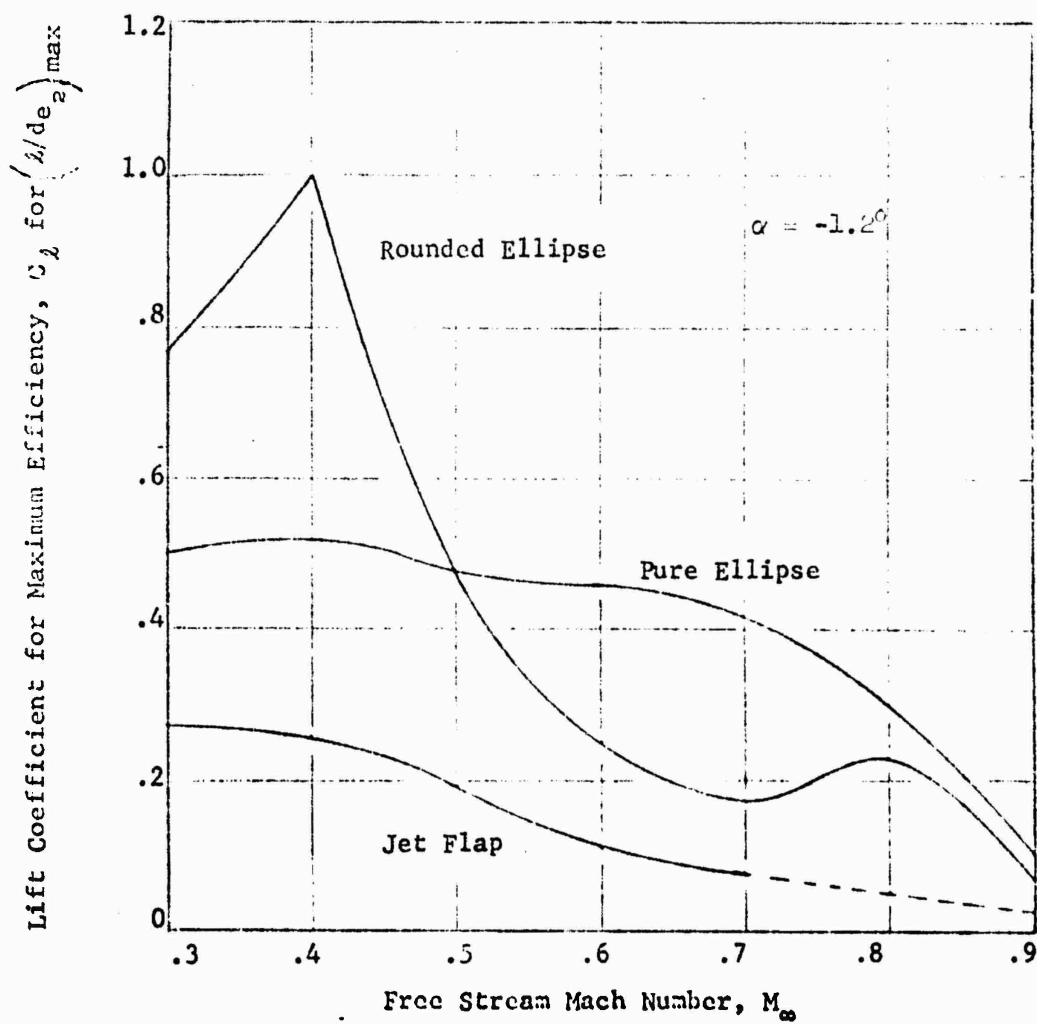The Three Configurations

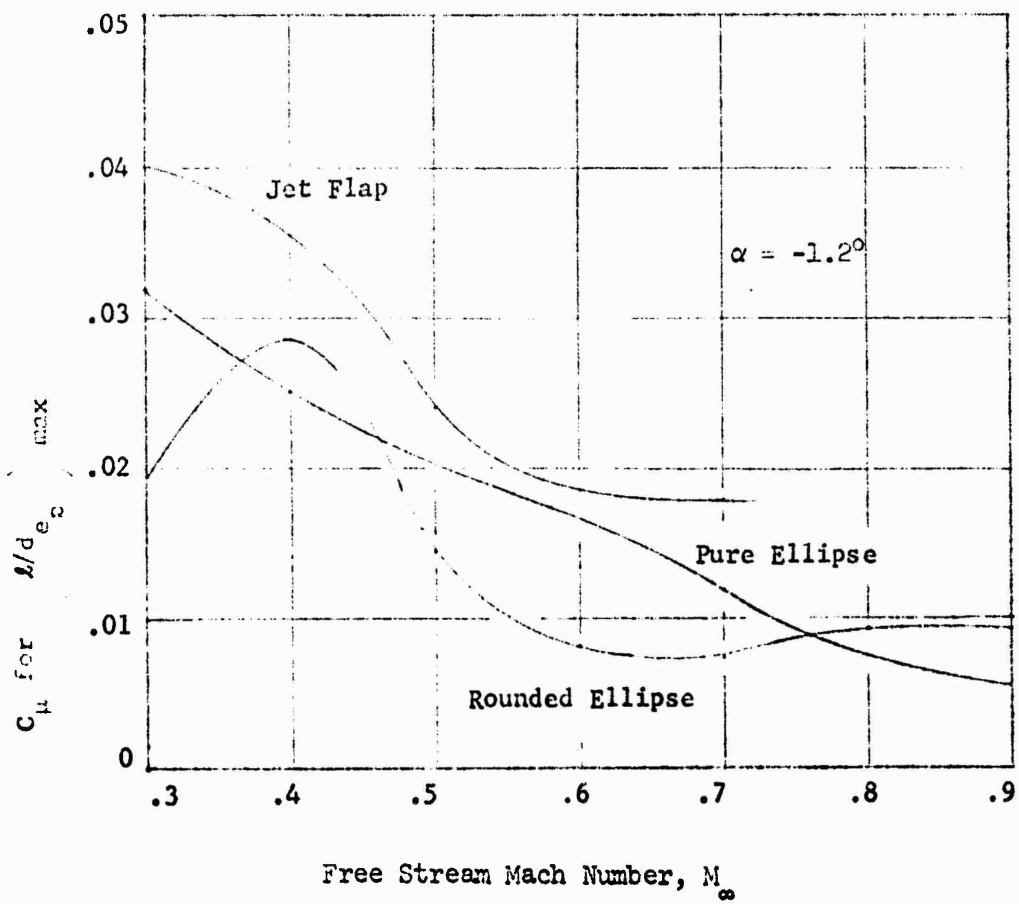**Figure 47 - Lift Corresponding to Maximum Aerodynamic Efficiency**

62

Figure 48 - Momentum Coefficients for Maximum
Aerodynamic Efficiencies

DOCUMENT CONTROL DATA - R & D

(Security classification of title, body of abstract and indexing annotation must be entered when the overall report is classified)

1. ORIGINATING ACTIVITY *(Corporate author)*	2a. REPORT SECURITY CLASSIFICATION
Aviation Department	UNCLASSIFIED
Naval Ship Research and Development Center	2b. GROUP
Washington, D.C. 20034	

3. REPORT TITLE

TWO-DIMENSIONAL TRANSONIC WIND TUNNEL TESTS OF THREE 15-PERCENT THICK
CIRCULATION CONTROL AIRFOILS

4. DESCRIPTIVE NOTES *(Type of report and inclusive dates)*

Technical Note

5. AUTHOR(S) *(First name, middle initial, last name)*

Robert J. Englar

6. REPORT DATE	7a. TOTAL NO. OF PAGES	7b. NO. OF REFS
December 1970	70	8

8a. CONTRACT OR GRANT NO.	9a. ORIGINATOR'S REPORT NUMBER(S)
b. PROJECT NO. AR 011 0101	Technical Note AL-182
c.	9b. OTHER REPORT NO(S) *(Any other numbers that may be assigned this report)*
NSRDC 635-673	

10. DISTRIBUTION STATEMENT

Distribution limited to U.S. Gov't agencies only; Test and Evaluation; December 1970.
Other requestes for this document must be referred to Naval Air Systems Command
(AIR320).

11. SUPPLEMENTARY NOTES	12. SPONSORING MILITARY ACTIVITY
	Naval Material Command (0314)
	Washington, D.C. 20360

13. ABSTRACT

Two-dimensional transonic wind tunnel tests were conducted on three fifteen
percent circulation control elliptic airfoils over the range $0.3 \leq M \leq 0.9$. Model
configurations included a pure elliptical shape with both jet flap and tangential
upper surface trailing edge blowing, plus tangential blowing over an elliptical
shape with a rounded trailing edge. Performance of the rounded trailing edge
configuration was the best of the three at low speeds, but above $M = 0.55$, detach-
ment of the Coanda jet caused rapid performance deterioration. Due to its elongated
trailing edge and associated larger effective radius downstream of the slot, the
tangentially blown pure ellipse was able to extend the jet detachment Mach number
to 0.7, where maximum equivalent lift-to-drag ratios of 22 at C_μ of 0.44 were

achieved. The jet flap proved to be inferior to the tangentially blown configu-
rations in all respects except in its ability as a thrusting, drag-reducing body.